Geomagnetic Disturbance Characterization in the Hydro-Quebec Power System using AUTUMNX Data

Submitted by

Manpreet Kaur (V00834213)

Bachelor of Technology, Electrical and Electronics Engineering,

Guru Gobind Singh Indraprastha University, 2012

A Report Submitted in Partial Fulfillment of the Requirement for the Degree of

Master of Engineering

in the Department of Electrical and Computer Engineering

University of Victoria

Supervisory Committee

Dr. T. Aaron Gulliver, Supervisor

(Department of Electrical and Computer Engineering)

Dr. Issa Traoré, Departmental Member

(Department of Electrical and Computer Engineering)

Abstract

A geomagnetic storm is a disturbance of the earth magnetosphere caused by a charged cloud of plasma (also known as solar wind) released after a solar flare event. The time varying magnetic field leads to an electric field which results in geomagnetically induced currents (GICs). These currents induced in power lines flow to ground via substation transformers which cause saturation of the transformer cores, leading to transformer damage. In addition, the harmonics induced in the power lines cause unwanted relay operations and trip power lines, which compromise the stability of the power system. Such events led to the famous Quebec blackout in Mar. 1989 which left the province without power for 9 hours.

According to Faraday's Law of Induction, the change in geomagnetic field is directly related to the electric field that induces the GICs. In [1] statistical models of the geomagnetic time derivative were developed and tested using data from the CANOPUS array of magnetometers. Empirical models for the log of the mean and log of the variance were used to predict extreme geomagnetic disturbances induced by solar wind. In this report, the results obtained in [1] are verified using over a year of AUTUMNX data which is about the same number of data values as the 10 years of CANOPUS data. An investigation of the effect of GICs on power systems is also presented. The geomagnetic data from the AUTUMNX array of magnetometers is related to harmonic data from the Hydro-Quebec power network. In the future, this can help Hydro-Quebec predict and prevent events like the 1989 blackout.

Table of Contents

List of Figures

List of Tables

Acknowledgements

I would like to thank my supervisor, Dr. T. Aaron Gulliver, for the patient guidance, encouragement, and advice he has provided throughout my time as his student. I have been extremely lucky to have a supervisor who cared so much about my work, and who responded to my questions and queries so promptly. I express my deepest gratitude to my work-term supervisor Prof. Martin Connors at Athabasca University for his constant support and guidance during this project, as well as the many rewarding discussions and comments. Furthermore, I thank Prof. Brian Jackel at the University of Calgary for sharing his ideas with me and helping me understand his work.

My extended thanks to Sebastien Guillon at Hydro-Quebec for answering all my queries related to the Hydro-Quebec data. I must also thank Kyle Reiter, Athabasca University and Mark J. Engebretson, Augsburg University, for their guidance and support. I take this opportunity to thank Dr. Issa Traoré and all the professors who taught me at UVic. Finally, I would like to thank and dedicate my work to the loving memory of my father for being my guiding star and always believing in me. I thank my mother and siblings for their selfless love, support and encouragement throughout my journey at the University of Victoria.

Dedicated to

My Parents and Family

Glossary

AUTUMNX – The Athabasca University Themis UCLA Magnetometer Network Extension (AUTUMNX) is a chain of 10 magnetometers installed in Quebec to monitor geomagnetic activity.

AUTUMNX magnetometer stations – There are 10 sites with magnetometers installed which are Salluit (SALU), Akulivik (AKUL), Puvirnituq (PUVR), Inukjuak (INUK), (Kuujjuarapik) KJPK, Radisson (RADI), Val-d'Or (VLDR), Saint-Felicien (STFL), Sept-Îles (SEPT) and Schefferville (SCHF).

CANOPUS – An array of magnetometers now called the Canadian Array for Realtime Investigations of Magnetic Activity (CARISMA) which is a component of the Geospace Observatory Canada project.

GMD – A geomagnetic disturbance (GMD) is a temporary disturbance of the earth's magnetosphere caused by solar wind (a charged cloud) released after a solar flare event.

GIC – Geomagnetically induced currents (GICs) are currents induced by GMD events.

Hydro-Quebec substations – The ten Hydro-Quebec substations considered in this report are Boucherville (BOU), Châteauguay (CHA), Chibougamau (CHI), Churchill Falls (CHU), La Grande 2 (LG2), Micoua (MIC), Nicolet (NIC), Outaouais (OUT), Rimouski (RIM) and Tilly (TIL).

SVC – A static VAR compensator is a high voltage system that dynamically controls the network voltage at its coupling point. The main task is to keep the network voltage constant at a set reference value.

IAGA– The International Association of Geomagnetism and Aeronomy

MACCS – The Magnetometer Array for Cusp and Cleft Studies (MACCS) project is a joint venture between the Augsburg College Physics Department and the Boston University Astronomy Department to study natural interactions in the earth's space environment.

Chapter 1: Introduction

1.1 Problem definition and motivation

Coronal mass ejections (CMEs) are clouds of plasma along with a strong magnetic field ejected from solar corona one to four days after a solar flare event. The charged particles from the sun interact with the earth's magnetic field and induce a geomagnetic storm. As a result, a geomagnetic disturbance (GMD) is observed on earth and intense GMDs cause the colorful aurora borealis or northern lights. The frequency of these disturbances varies with the average sunspot cycle of approximately 11 years. GMDs lead to very low-frequency quasi-direct currents called geomagnetically induced currents (GICs). GICs are undesirable as they adversely affect air traffic control systems, pipes, railroads and power systems [2].

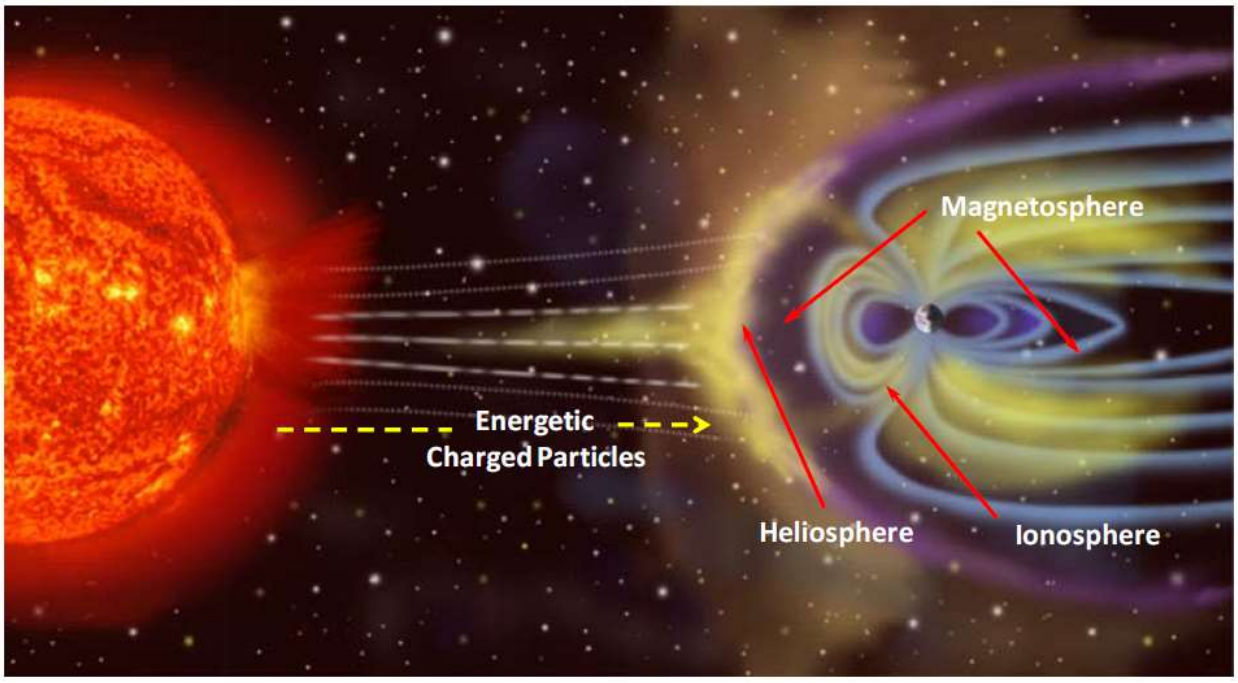

Figure 1.1: A coronal mass ejection event showing the plasma cloud ejected from the solar surface interacting with the earth's magnetic field [3].

1.2 Impact of geomagnetically induced currents

The major and most direct impact of GICs is on power systems. As rock is not a good conductor of electricity and has high resistance, GICs on the surface of earth tend to flow in low resistance high voltage power transmission lines. GICs flowing through transformer windings produce extra magnetization which can saturate the core of the transformers. This saturation leads to spikes in the AC waveform which increases harmonics and jeopardizes power system integrity by unnecessarily activating relays and other equipment. This can result in problems ranging from individual power lines tripping to the collapse of the power system. In addition, saturation of the transformer cores produces extra eddy currents which overheat the transformers. This may not affect the overall core temperature but localized hot spots can damage the transformer windings [4].

All power systems located at higher latitudes such as in Scandinavia, Alaska, northern Russia, and Quebec are vulnerable to the effects of a geomagnetic storm. The failure of power transformers during Mar. 2001 in South Africa, the blackout in Sweden during Oct. 2003 and the Mar. 1989 Hydro-Quebec blackout are just some of the results of extreme GMDs. Quebec is highly susceptible to GICs because of the large Canadian Shield which prevents currents from easily flowing through the ground. In addition, the long length of Hydro-Quebec transmission lines increases their vulnerability.

1.3 The 1989 Hydro-Quebec blackout

On Mar. 13, 1989, Hydro-Quebec had a massive blackout due to a geomagnetic storm. The variations in the earth's magnetic field tripped circuit breakers in the Hydro-Quebec power system, resulting in a blackout that lasted 9 hours. In monetary terms, this blackout cost Hydro-Quebec about $13.2 million of which $6.5 million was damaged equipment. Figure 1.2 shows the magnitude of the magnetic field due to the geomagnetic storm in one minute increments. The most magnetically active region with a magnetic field on the order of 400 nanoTesla (nT) per minute is shown in red and is located in Quebec.

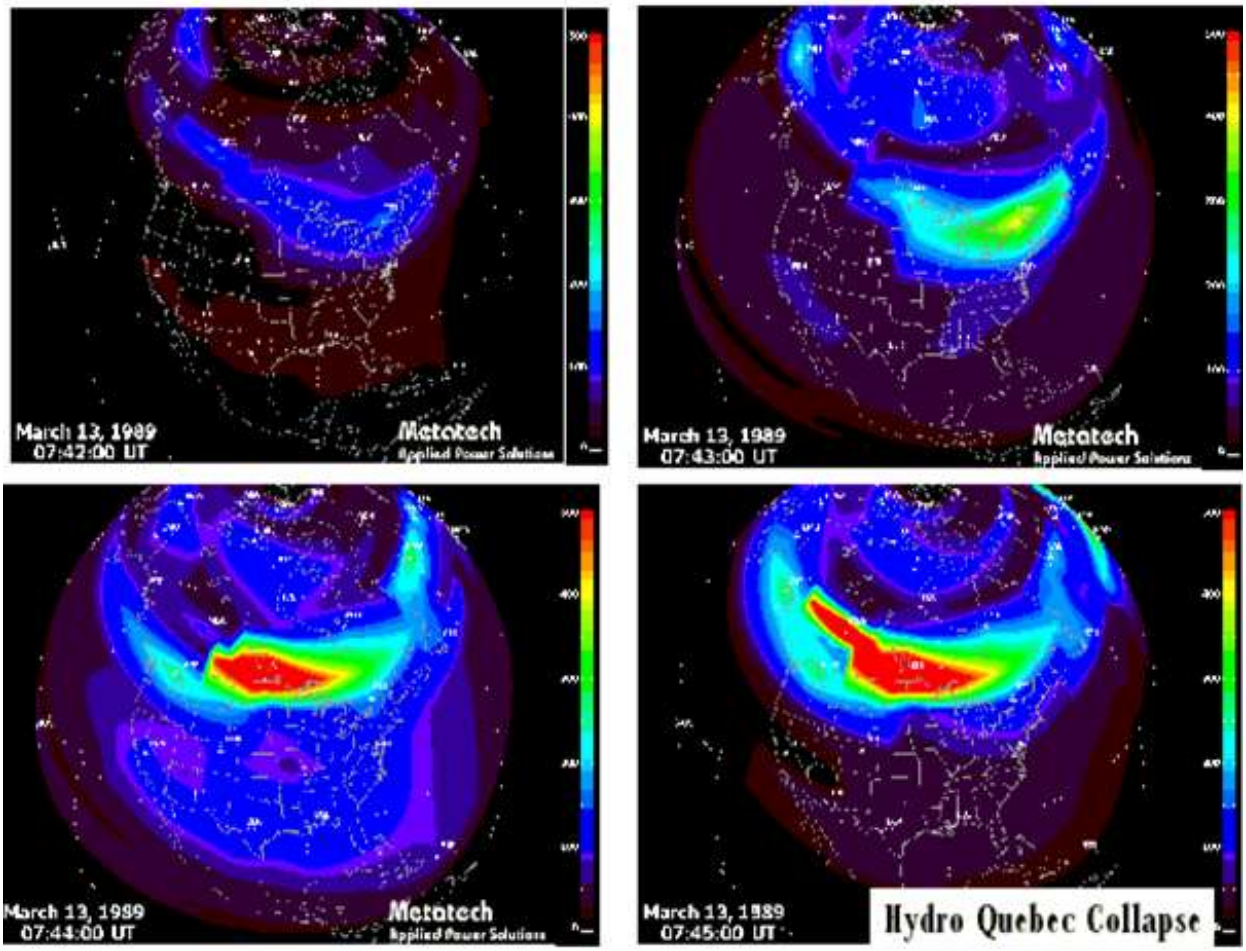

Figure 1.2: The magnitude of the 1989 geomagnetic storm that led to the Hydro-Quebec power system collapse. Red indicates a magnitude of 400 nT per minute which is over Quebec [5].

Figure 1.3 shows the series of events in order of occurrence on the Hydro-Quebec network that led to the blackout. The first static VAR compensator (SVC) tripped at 2:22:17 AM in

Chibougamau (location 1), followed by SVCs tripping at locations 2, 3 and 4. At 02:45:25 AM, all five 735 KV lines tripped out. This was followed by the Churchill Falls generation separation and finally the system collapse at 2:45:49 AM.

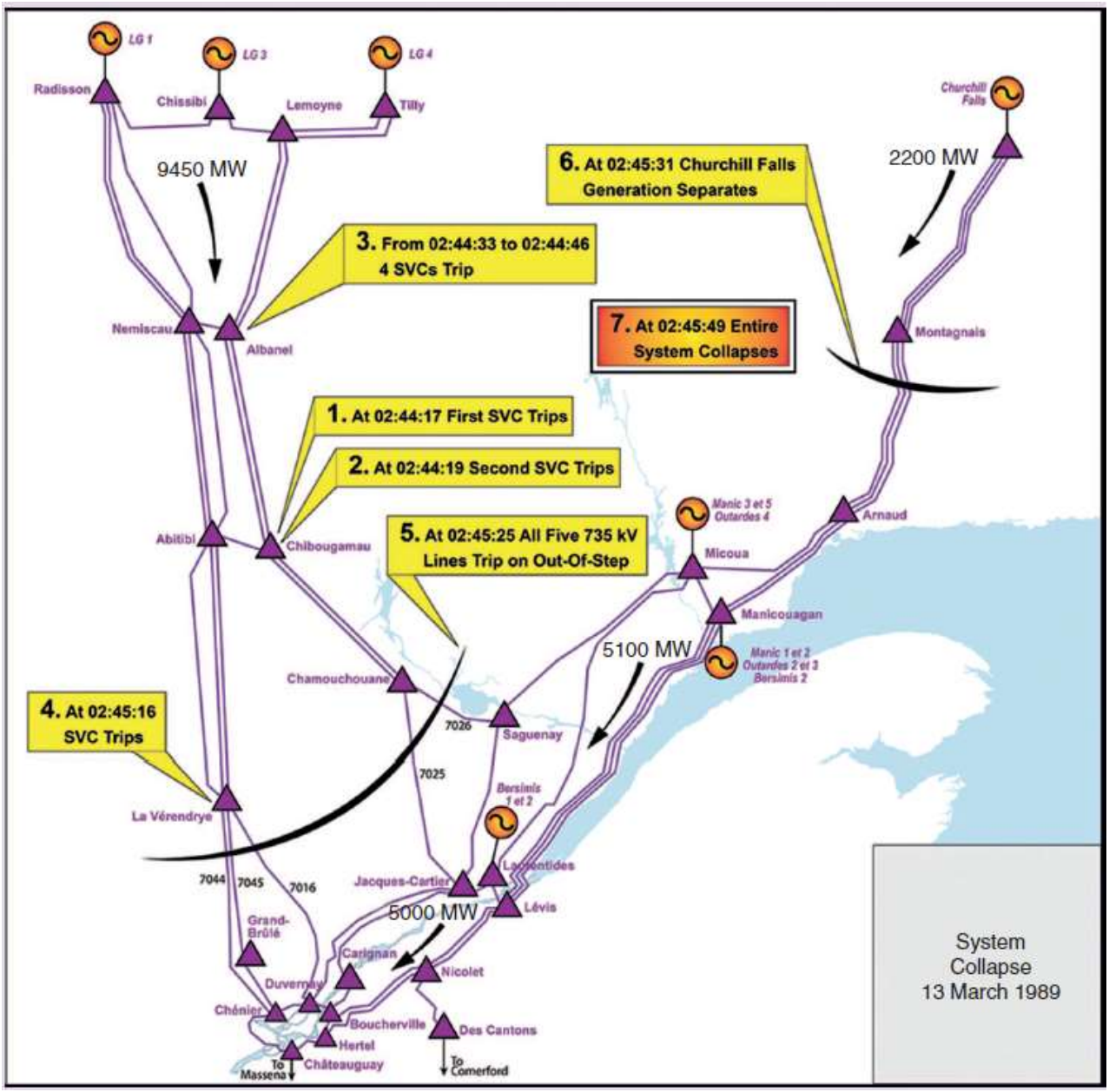

Figure 1.3: The series of events that led to the 1989 Hydro-Quebec power system collapse [6].

In the years following the 1989 blackout, various mitigation techniques such as series compensation were developed to reduce the likelihood of a blackout happening again. Series

compensation uses capacitors connected in series with a transmission line to regulate the voltage. This provides a high-impedance path for GICs and redistributes GICs in the network [7].

Monitoring GMDs is important for effective mitigation of the associated risks. Hence, arrays of magnetometers have been installed by various research organizations [8]. A magnetometer measures geomagnetic activity, which can be related to solar activity. The AUTUMN Extension (AUTUMNX) is an array of 10 magnetometers installed in Quebec to monitor the change in magnetic field, denoted as *dB/dt*. AUTUMNX is funded through the Canadian Space Agency and Geospace Observatory Canada and run by a research team at Athabasca University. These magnetometers provide a large amount of geographically dispersed magnetic field data from Quebec.

The geomagnetically induced currents (GICs) produced in power systems during geomagnetic storms are a function of the electric field amplitude and direction, and the characteristics of the power system. According to Faraday's Law of Induction, $\nabla \times \vec{E} = -\frac{\partial \vec{B}}{\partial t}$ where B denotes the magnetic field and E denotes the electric field, a changing magnetic field density through a defined area, or a changing flux, results in an induced electromotive force (EMF). In this report, the EMF is the result of a geomagnetic storm interacting with the earth's magnetic field which induces electric fields at the earth's surface and in the ground. This creates quasi-DC currents in high voltage transmission lines, railway equipment, communication cables, and pipes. These currents produce harmonics in transmission lines. The AUTUMNX magnetometer data can provide information about the harmonics in Hydro-Quebec power lines. In this report, AUTUMNX magnetometer data is compared with Hydro-Quebec harmonic data to determine the relationship between them. The AUTUMNX data is examined to eliminate false data due to unnatural events or activities, e.g. a vehicle passing nearby. The analysis of the remaining data will enable Hydro-Quebec to understand the effects of geomagnetic activity on their power system and develop proper mitigation techniques.

In [1], the rate of change of the magnetic field (*dB/dt*) was studied using the CANOPUS magnetometer array data for the Gillam station. An empirical model was developed for the distribution of the geomagnetic time derivative *dB/dt* as a function of solar wind conditions and local magnetic activity. The main finding was that *dB/dt* can be divided into a portion having a

very short correlation time called the variability and another portion with a relatively longer correlation time called the intensity. A goal of this report is to verify the results in [1] using about a year of AUTUMNX data, which is approximately the same number of data points as the 10 years of CANOPUS data with a sampling rate of 0.2 Hz since the AUTUMNX sampling rate is 2 Hz. The analysis is performed for all AUTUMNX stations to compare the data between them.

1.4 Report structure

In this report, the results obtained based on the CANOPUS data for the Gillam station in [1] are compared with the AUTUMNX data for the SALU station. Furthermore, the AUTUMNX data is characterized and compared to the Hydro-Quebec harmonic data. The remainder of this report is organized as follows. In Chapter 2, a statistical analysis of the AUTUMNX data is presented. The *dB/dt* results for various stations are compared in Section 2.3 to determine the characteristics of GMDs. Some of the major events corresponding to solar activity are discussed based on the variations observed in the Hydro-Quebec harmonic data and the AUTUMNX *dB/dt* data. In Chapter 3, a summary of the results is given along with suggestions for future work.

Chapter 2: Analysis and results

The AUTUMNX website provides magnetometer data from 10 stations in near real time. Figure 2.1(a) shows the geomagnetic field *B* plots versus time for the three directional components *X*, *Y*, and *Z* for Jan. 8, 2017. *B* in nanoTesla (nT) is on the *Y*-axis and time (UTC hours) is on the *X*-axis. This figure gives results for four sites, Salluit (SALU), Puvirnituq (PUVR), Inukjuak (INUK) and Kuujjuarapik (KJPK) out of the 10 magnetometer sites of the AUTMNX array. The other 6 sites are Akulivik (AKUL), Radisson (RADI), Val-d'Or (VLDR), Saint-Felicien (STFL), Sept-Îles (SEPT) and Schefferville (SCHF). AUTUMNX data is available for dates since its installation in Oct. 2014.

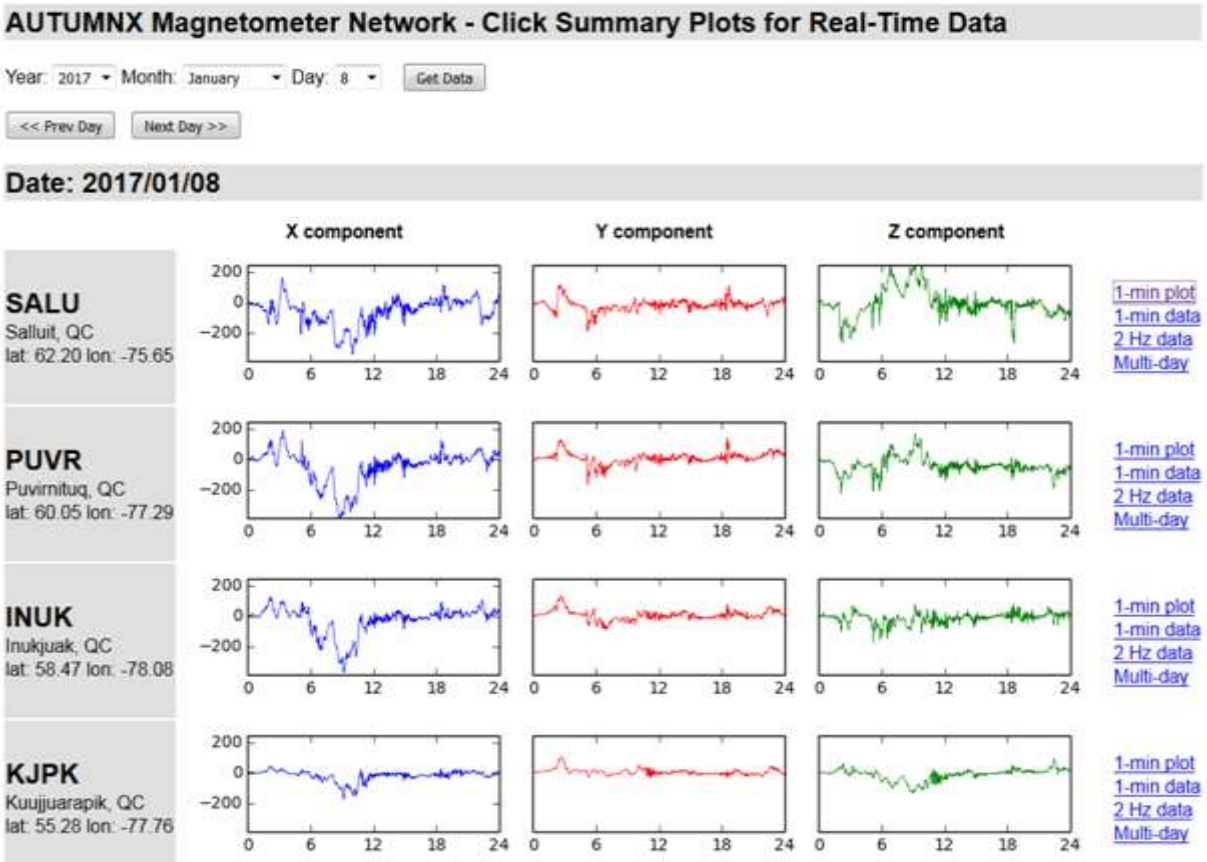

Figure 2.1(a): AUTUMNX summary plots for the magnetometer data versus time (UTC hours) [9].

Figure 2.1(b) shows the geomagnetic field data for the SALU station for Jan. 8, 2017 along with the day and time stamp in International Association of Geomagnetism and Aeronomy (IAGA)-2002 format. This format is intended as a data exchange format for geomagnetic data from observatories at time intervals from millisecond up to and including monthly means [10]. In this figure, SALUH, SALUD and SALUZ are the geomagnetic field *B* values for the *X*, *Y* and *Z* components in nT. DOY is the day of the year and SALUF does not have any significance for this study and so can be ignored. This figure also contains the latitude and longitude information of the SALU station and the data sampling rate which is 2 Hz.

Format	IAGA-2002					
Source of Data	Ath. Univ. THEMIS UCLA Magnetic Network eXpan					
Station Name						
IAGA CODE	SALU					
Geodetic Latitude	62.20					
Geodetic Longitude	-75.63					
Reported	HDZF					
Sensor Orientation	HDZF					
Elevation	227					
Digital Sampling	0.5					
Data Interval Type	0.5-second instantaneous					
Data Type	Variation					
DATE	TIME	DOY	SALUH	SALUD	SALUZ	SALUF
2015-12-07	00:00:00.412	341	10346.51	-155.00	58009.23	88888.00
2015-12-07	00:00:00.912	341	10346.48	-155.00	58009.53	88888.00
2015-12-07	00:00:01.412	341	10346.35	-155.06	58009.55	88888.00
2015-12-07	00:00:01.912	341	10346.36	-155.35	58009.69	88888.00
2015-12-07	00:00:02.412	341	10345.82	-156.11	58009.88	88888.00
2015-12-07	00:00:02.912	341	10345.65	-156.40	58010.20	88888.00
2015-12-07	00:00:03.412	341	10345.42	-156.69	58010.39	88888.00
2015-12-07	00:00:03.912	341	10345.40	-156.87	58010.50	88888.00
2015-12-07	00:00:04.412	341	10345.34	-157.17	58010.59	88888.00
2015-12-07	00:00:04.912	341	10345.28	-157.31	58010.41	88888.00
2015-12-07	00:00:05.412	341	10345.08	-157.73	58010.82	88888.00
2015-12-07	00:00:05.912	341	10344.76	-158.20	58011.10	88888.00
2015-12-07	00:00:06.412	341	10344.47	-158.34	58011.20	88888.00
2015-12-07	00:00:06.912	341	10344.42	-158.45	58011.54	88888.00
2015-12-07	00:00:07.412	341	10344.29	-158.63	58011.81	88888.00
2015-12-07	00:00:07.912	341	10343.96	-159.00	58011.99	88888.00
2015-12-07	00:00:08.412	341	10343.65	-159.21	58012.30	88888.00

Figure 2.1(b): SALU data for Jan. 8, 2017 in IAGA-2002 format from the AUTUMNX website [9].

Figure 2.2 shows an AUTUMNX magnetometer. At the bottom is an uninterrupted power supply (UPS), in the middle is a network control center and at the top is a Beagleboard computer and THEMIS magnetometer control box. An antenna is used on top of the unit at some sites for better reception. Figure 2.3 shows the location of the magnetometers in eastern Canada. The AUTUMNX array is indicated with yellow dots, the THEMIS network magnetometers with green dots, the NRCan CANMOS magnetometers with red dots, the Magnetometer Array for Cusp and Cleft Studies (MACCS) with dark brown dots, and the future site of NRCan Fredericton with a light brown dot. The Hydro-Québec electrical transmission system is outlined with red lines [11].

Figure 2.2: An AUTUMNX ground-based observation unit [11].

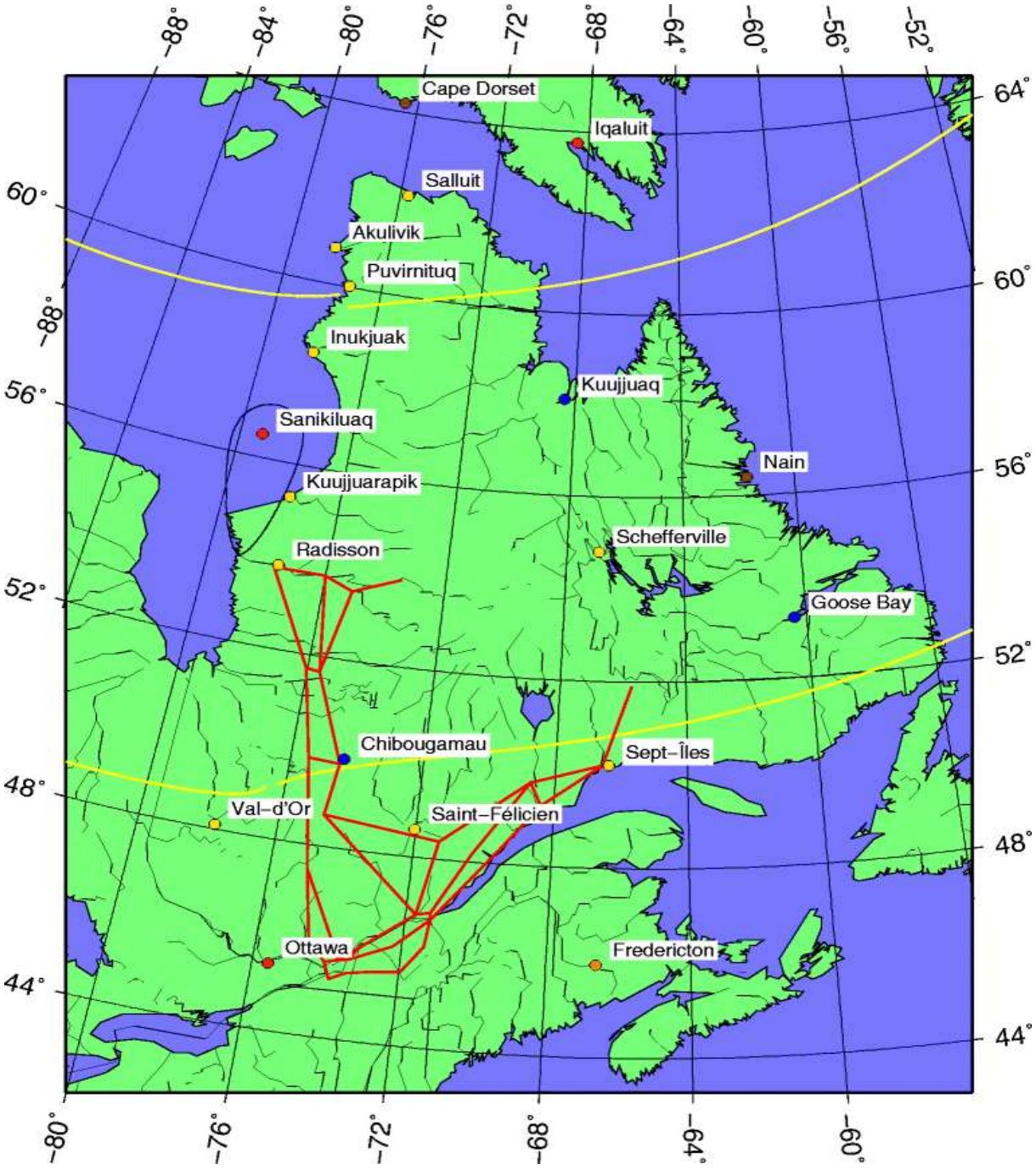

Figure 2.3: The locations of the magnetometers in Quebec including the AUTUMNX array as well as the other magnetometers in eastern Canada. The AUTUMNX array is indicated by yellow dots [11].

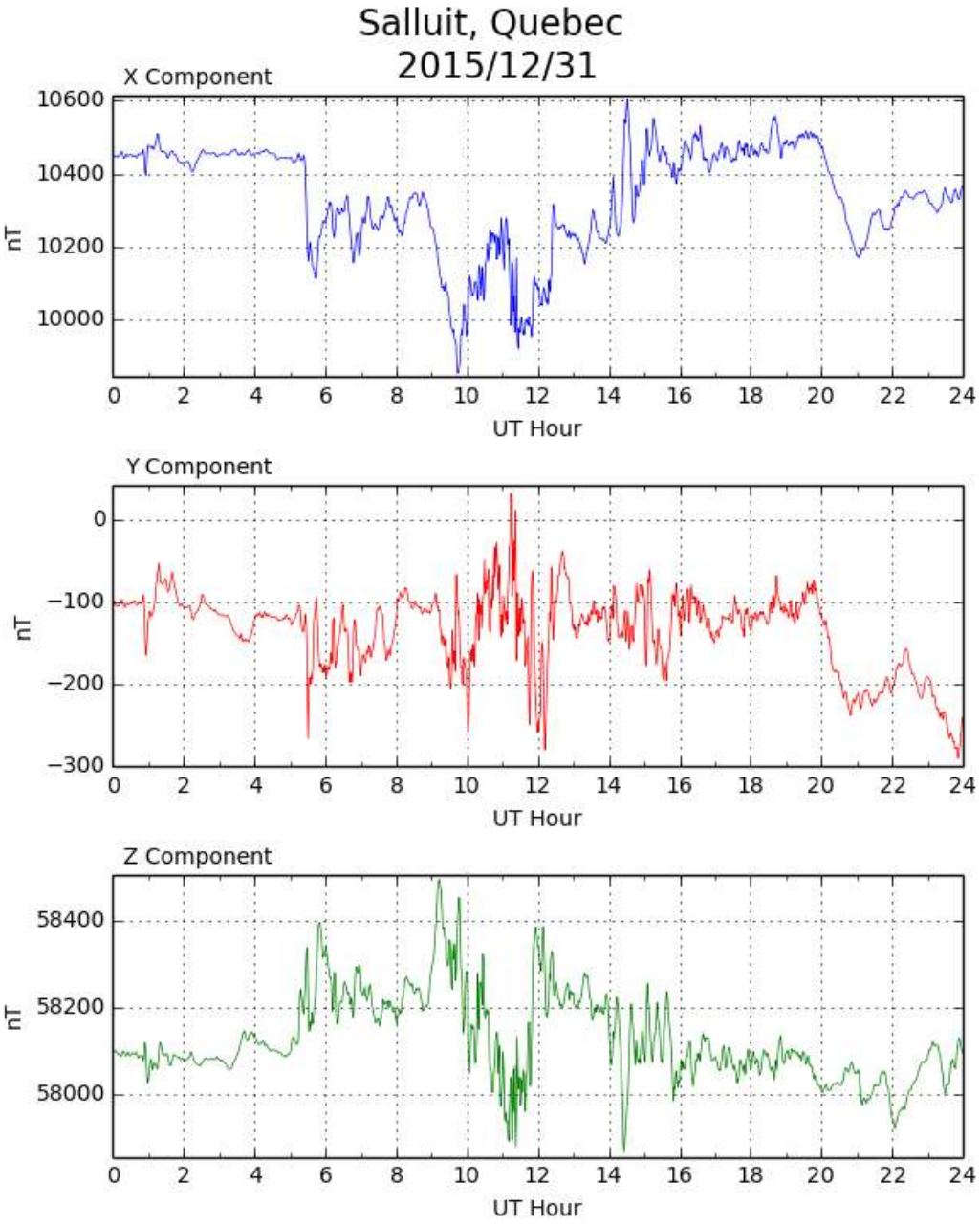

Figure 2.4: One day (00-24 hours UT Dec. 31, 2015) of magnetometer data from the SALU station showing the *X*, *Y*, and *Z* components of the geomagnetic field *B* [9].

Figures 2.4 and 2.5 show the magnetometer data for a geomagnetically calm day and a relatively active day for the SALU station, respectively. A geomagnetically active day has sudden fluctuations of over 500 nT as indicated in Figure 2.5. The spikes in the magnetic field of around 600 nT around 1:40 AM are the result of a geomagnetic storm.

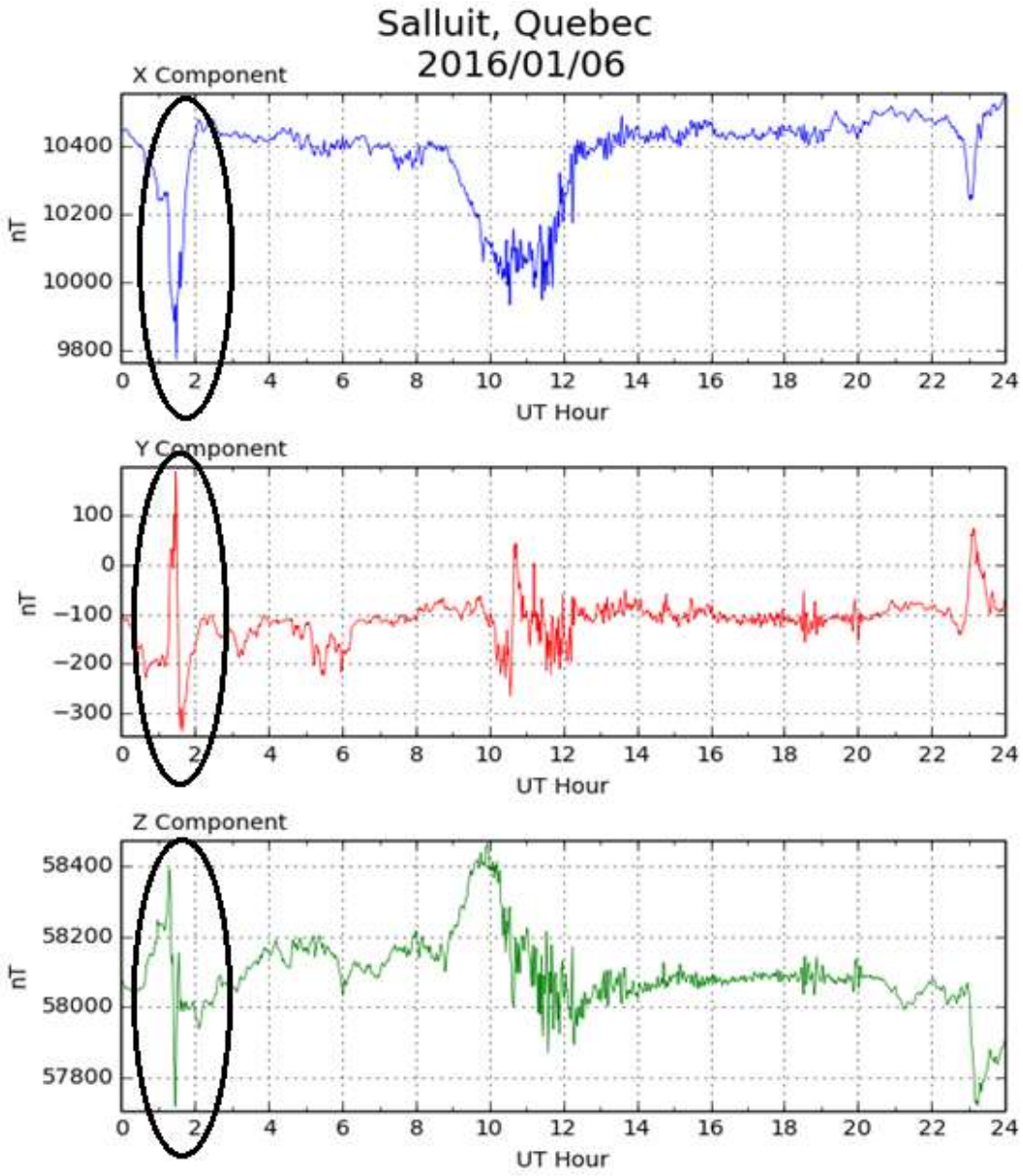

Figure 2.5: Magnetometer data (00-24 hours UT Jan. 6, 2016) for the SALU station showing the *X*, *Y* and *Z* components of the magnetic field. The spikes at 1:40 AM are due to a geomagnetic storm [9].

2.1 Analysis of 24 hours (one day) of data

Data from the SALU station for a randomly chosen magnetically calm day Dec. 31, 2015. The vector time derivative of the magnetic field was calculated using the difference between successive time samples. The instantaneous values for the three directional components of the derivative of *B* are given by

$$d\vec{B}_X\,/dt \;\approx\; \frac{\vec{B}_X(t+\Delta t)-\vec{B}_X(t)}{\Delta t}$$

$$d\vec{B}_Y/dt \;\approx\; \frac{\vec{B}_Y(t+\Delta t)-\vec{B}_Y(t)}{\Delta t}$$

$$d\vec{B}z/dt \;\approx\; \frac{\vec{B}_Z(t+\Delta t)-\vec{B}_Z(t)}{\Delta t}$$

where t is time and Δt is the difference between successive time values, which here is 0.5 sec. It is assumed that X changes from negative to positive moving east to west, Y changes from negative to positive moving south to north and positive Z is out of the XY plane and negative Z is into the XY plane. The vector derivatives of B were then converted to scalars using

$$|dB/dt| \;=\left(\left(\frac{d\vec{B}_X}{dt}\right)^2+\left(\frac{d\vec{B}_Y}{dt}\right)^2+\left(\frac{d\vec{B}_Z}{dt}\right)^2\right)^{\frac{1}{2}} \qquad (1)$$

Figure 2.6 shows the $|dB/dt|$ values on a linear scale for the Gillam station in the CANOPUS array and Figure 2.7 shows the values on a log scale. This geomagnetic activity is a combination of rapid fluctuations superimposed on a more slowly varying progression. The fluctuations observed usually fall inside an envelope with a nearly constant range. Thus, the geomagnetic activity on a log scale can be expressed in terms of variability corresponding to the fluctuation envelope and the average referred to as intensity [1].

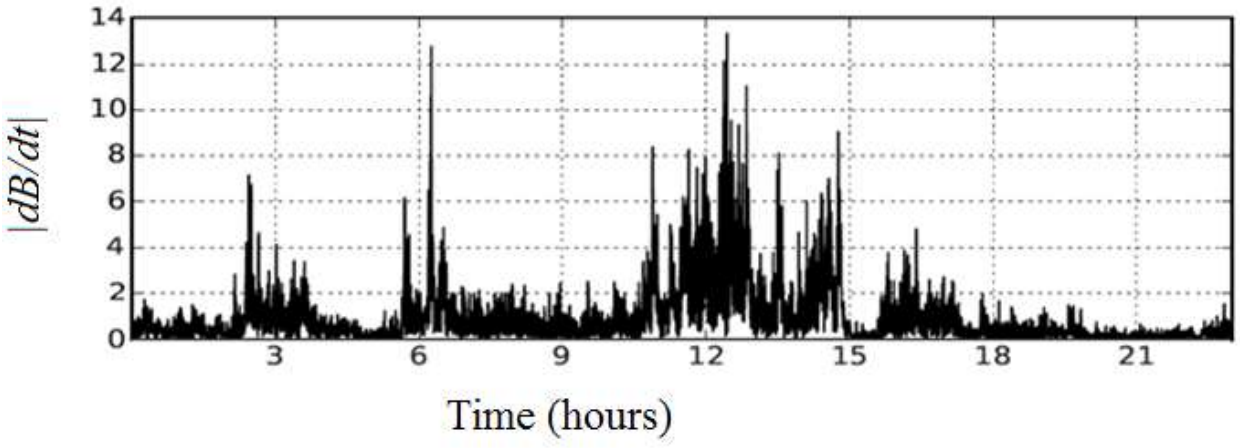

Figure 2.6: Magnitude of |*dB/dt*| on a linear scale for 24 hours (Apr. 2, 2000) at the Gillam station of the CANOPUS array [1].

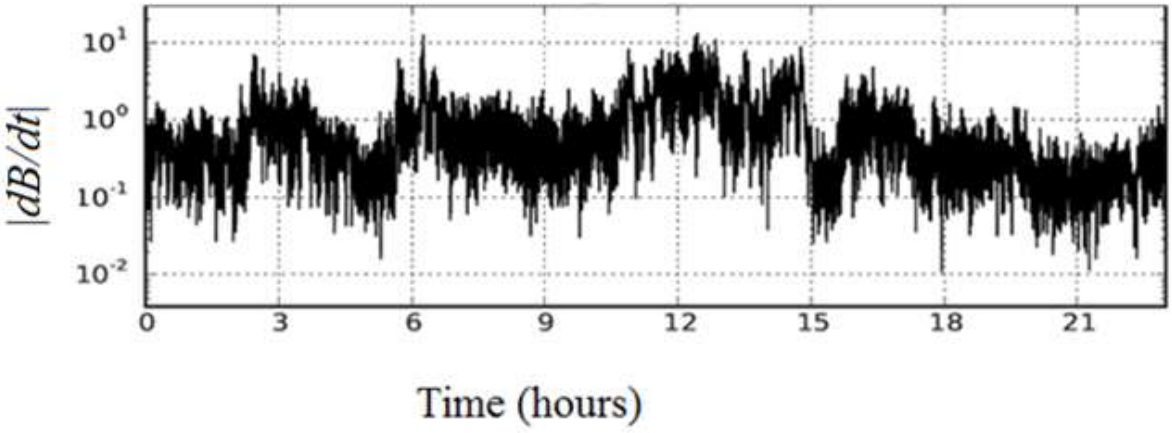

Figure 2.7: Magnitude of |*dB/dt*| on a log scale for 24 hours (Apr. 2, 2000) at the Gillam station of the CANOPUS array [1].

2.1.1 Lognormality

The change in magnetic activity $|dB/dt|$ on a logarithmic scale for the SALU station on Dec. 31, 2015 is shown in Figure 2.8. The values on the far left reflect magnetometer limitations and can be ignored [1]. The distribution of |*dB/dt*| is well approximated using a parabola in log-log coordinates which corresponds to a lognormal distribution in linear coordinates [1].

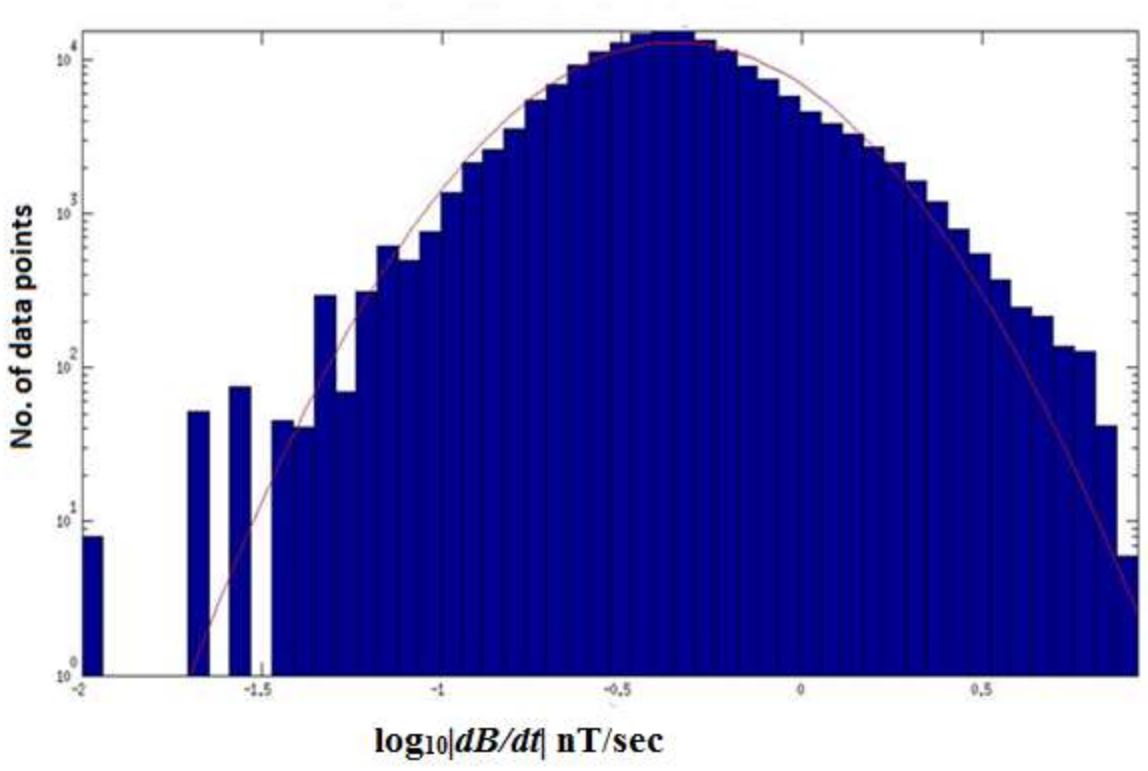

Figure 2.8: Histogram of $\log_{10}|dB/dt|$ for Dec. 31, 2015 with the best-fit lognormal distribution for the SALU station.

For a sequence of N vector magnetic field measurements, the instantaneous geomagnetic activity is defined as

$$M_n = \log_{10} \left|\frac{dB_n}{dt}\right|, n=1, 2, 3,\ldots, N\text{-}1 \qquad (2)$$

For a 24 hour day and a sampling rate of 0.5 sec, N=24×60×60×2=172800. The lognormal distribution L is

$$L = \frac{1}{x\,\sigma(2\pi)^{\frac{1}{2}}} e\left\{\frac{-(\ln x-\mu)^2}{2\sigma^2}\right\} \qquad (3)$$

where μ and σ are the mean and standard deviation of M, x>0, -∞< μ <∞ and $\sigma \geq 0$ [12].

The intensity I and variability V are defined as

$$I = \frac{1}{N-1}\sum_{n=1}^{N-1} M_{\mathrm{n}} \qquad (4)$$

and

$$V = \sqrt{(\frac{1}{N-2}\sum_{n=1}^{N-1} (M_{\mathrm{n}} - I)^2)} \qquad (5)$$

If the data have an approximately lognormal distribution, then I ≈ μ and $V \approx \sigma$, so these values are used in this report. The corresponding best-fit lognormal distribution using (3) is shown as a dashed red line in Figure 2.8. Figure 2.9 shows the intensity (mean of geomagnetic activity) in green and variability (standard deviation of geomagnetic activity) in blue versus time (24 hours). The intensity and variability of the $|dB/dt|$ data are calculated for 2.5 minute intervals which gives 576 values per day. This figure shows that the intensity changes by a factor of 20 while the variability is approximately constant, which suggests that these two quantities are approximately independent measures of geomagnetic activity. As the geomagnetic activity is high, sharp peaks are seen in Figure 2.9. In order to study the magnetic activity, a similar approach to [1] is used. In [1] statistical models of the geomagnetic time derivative were developed and tested using data from the CANOPUS array of magnetometers. Empirical models for the log of the mean and log of the variance were used to predict extreme geomagnetic disturbances induced by solar wind. In this report, results were generated using MATLAB for data from the SALU station of the AUTUMNX array.

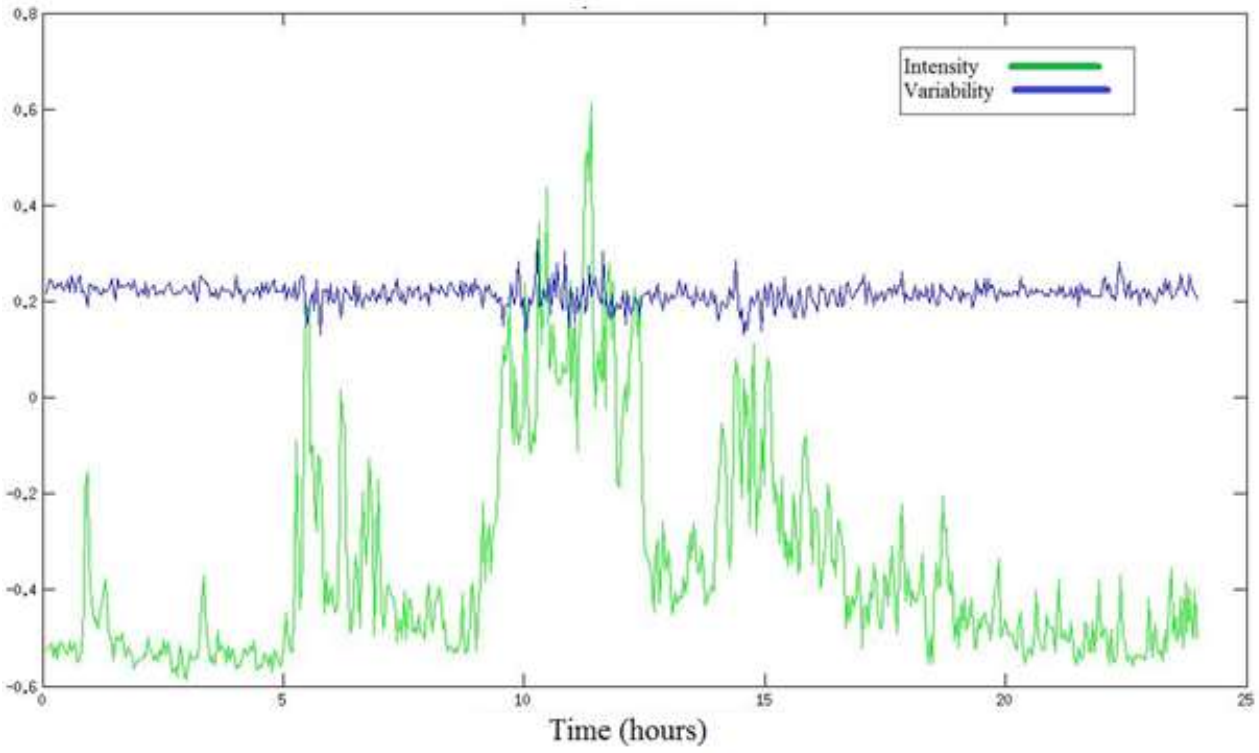

Figure 2.9: Mean and standard deviation of $\log_{10}|dB/dt|$ calculated using 2.5 minute intervals over a day. The variability (standard deviation of $\log_{10}|dB/dt|$) has a nearly constant average, while significant variations are seen in the intensity (mean of $\log_{10}|dB/dt|$)

2.1.2 Autocorrelation

Autocorrelation is a measure of the similarity between a sequence and a lagged version of the sequence. The autocorrelation can range from +1 to -1. An autocorrelation of +1 represents an exact positive correlation. An autocorrelation of -1, on the other hand, represents an exact negative correlation [13].

The autocorrelation for lag k is $r_k = \frac{c_k}{c_0}$ where

$$c_k = \frac{1}{J}\sum_{j=0}^{J-1}(s_j - \bar{s})\left(s_{(j+k)\text{modulo } K} - \bar{s}\right), \; k = 0, 1, \ldots, K\text{-}1 \qquad (6)$$

where J is the length of the sequence, K-1 is the maximum lag, $s_{(j+k)\text{modulo}\,K}$ is the circular shift in the lagged sequence, c_0 is the variance and $\bar{s}$ is the mean of the sequence s. The autocorrelation of the intensity and variability are calculated using 2.5 minute intervals of data so that J=24×60/2.5=576 samples/day [14]. In this report, the cyclic autocorrelation of intensity and variability is presented for a lag of 0 to K-1=99. The autocorrelation of the intensity and variability differ significantly, as shown in Figure 2.10. Intensity is highly correlated at small lags and is consistent with timescales of an hour. On the other hand, the variability is nearly uncorrelated at any lag. These results suggest that the intensity is smooth while the variability fluctuates.

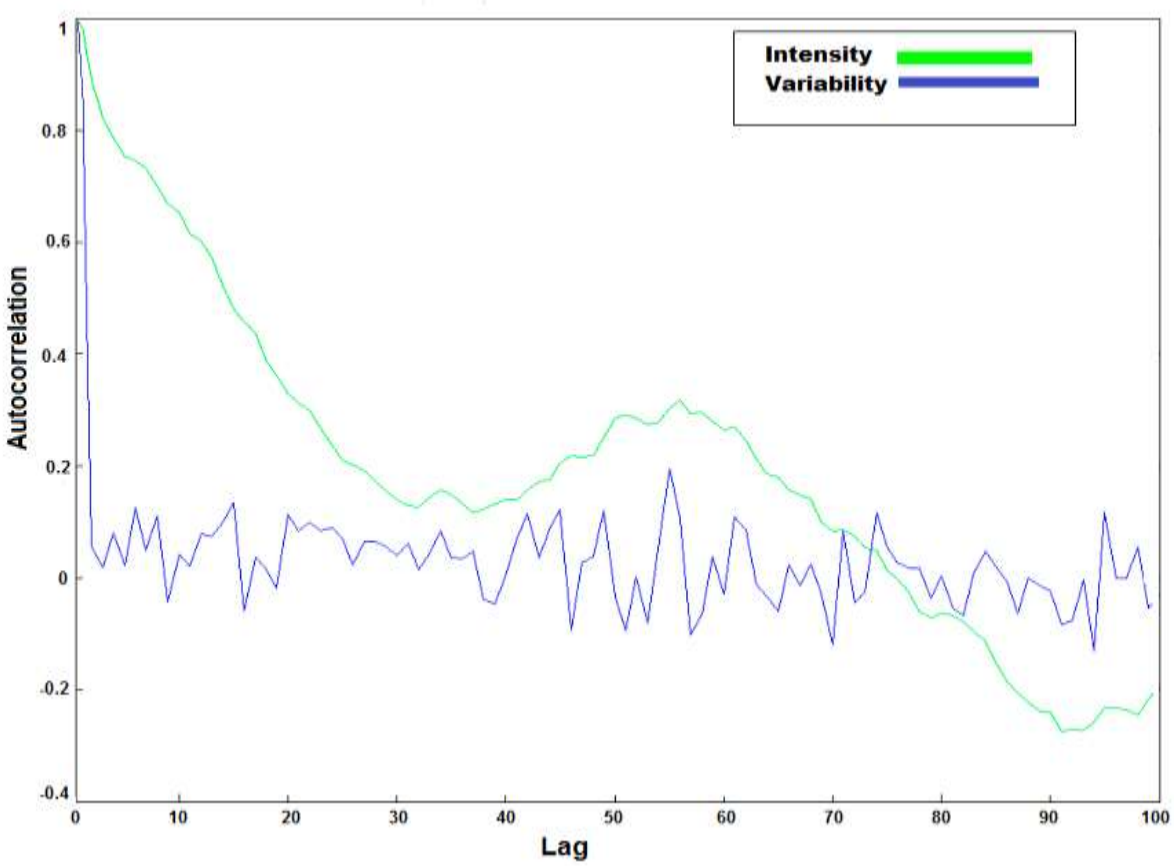

Figure 2.10: The autocorrelation of the intensity and variability versus time (24 hours) calculated over 2.5 minute intervals. The variability has a very negligible correlation time (< 5 minutes), while the intensity is correlated over timescales of tens of minutes to hours. Autocorrelation of the intensity (mean) is in green and the variability (standard deviation) is in blue.

2.2 Analysis of $\log_{10}|dB/dt|$ for Oct. 4, 2014 to Dec. 22, 2015

The MATLAB program used data from .txt files as given in Figure 2.1(b) for Oct. 4, 2014 to Dec. 22, 2015. These data files were downloaded from the AUTUMNX website for each day and used to produce histograms of $\log_{10}|dB/dt|$ for the specified duration. Figure 2.11 gives the histogram of $\log_{10}|dB/dt|$ for the KJPK station prior to the removal of erroneous data. Here, values of 10 or greater are considered to be due to errors when a vehicle passes near the magnetometer giving rise to false spikes. Magnetometer reset is another source of error that can skew the distribution.

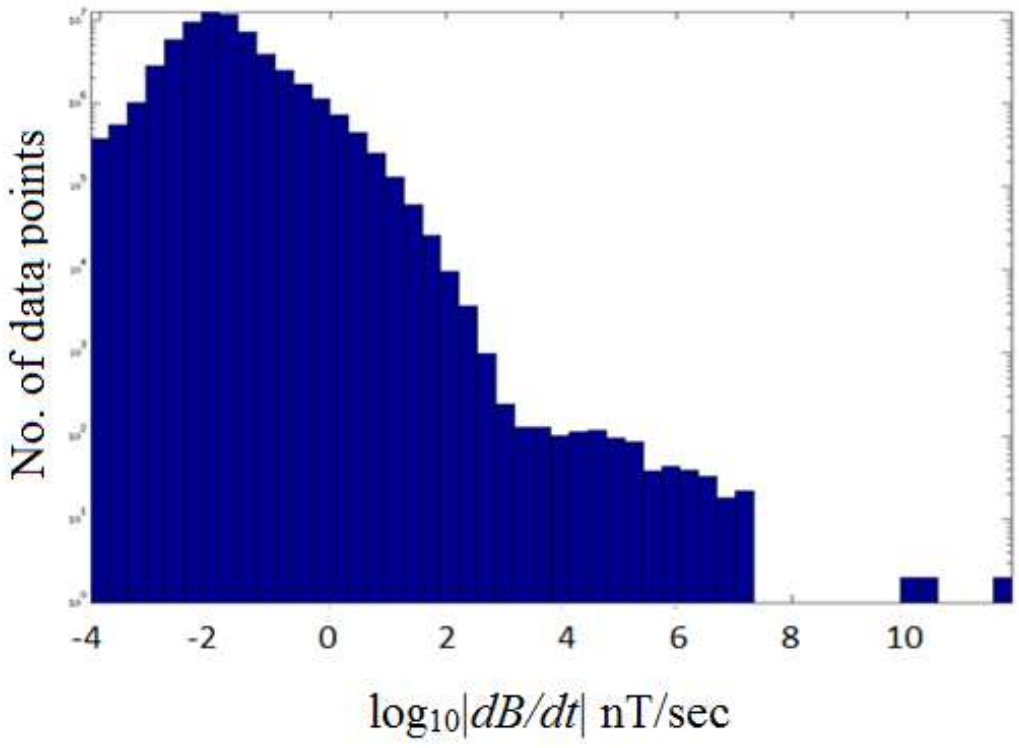

Figure 2.11: Histogram of $\log_{10}|dB/dt|$ with some erroneous data for the KJPK station.

Figures 2.12 to 2.21 give the histograms of $\log_{10}|dB/dt|$ for the AUTUMNX stations (except RADI) after discarding the erroneous data. More than half of the data for the RADI station was erroneous, hence it was not used for this study. Values on the far right of the histograms can be studied to identify GMD events. This will help determine the extreme geomagnetic events during the time period about a year. Values on the right that do not fit under the best-fit lognormal distribution are considered to be due to GMDs.

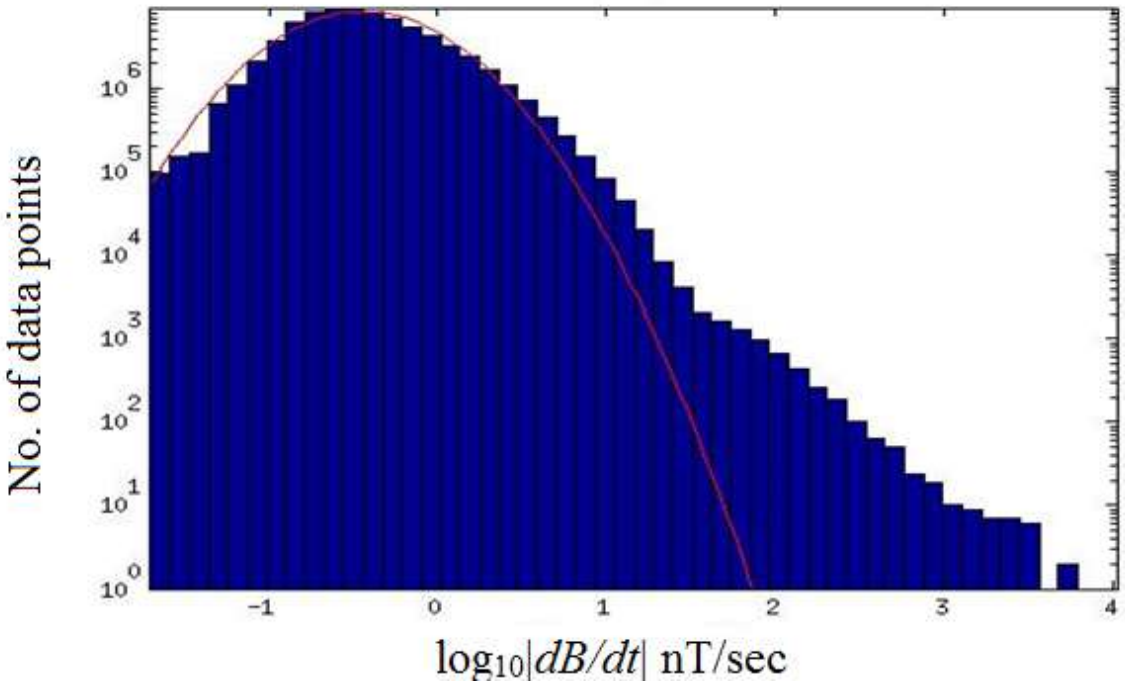

Figure 2.12: Histogram of $\log_{10}|dB/dt|$ for the AKUL station with the best-fit lognormal distribution.

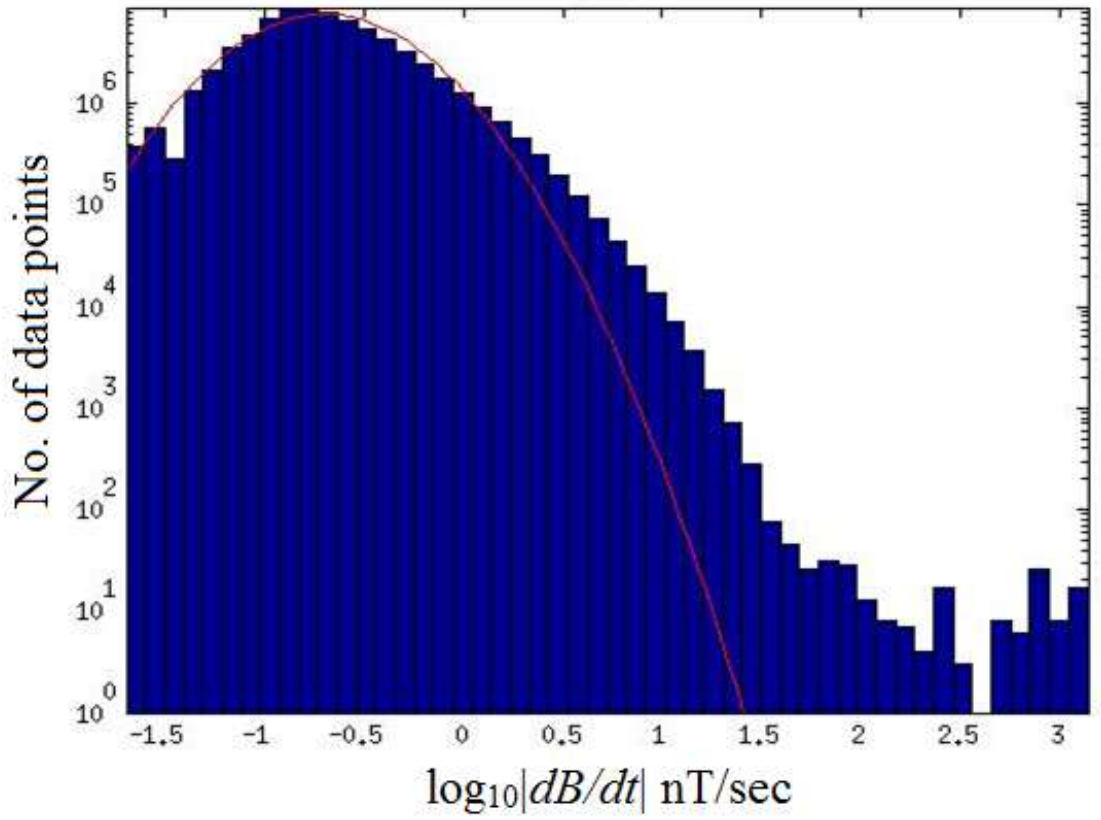

Figure 2.13: Histogram of the INUK $\log_{10}|dB/dt|$ data with the best-fit lognormal distribution.

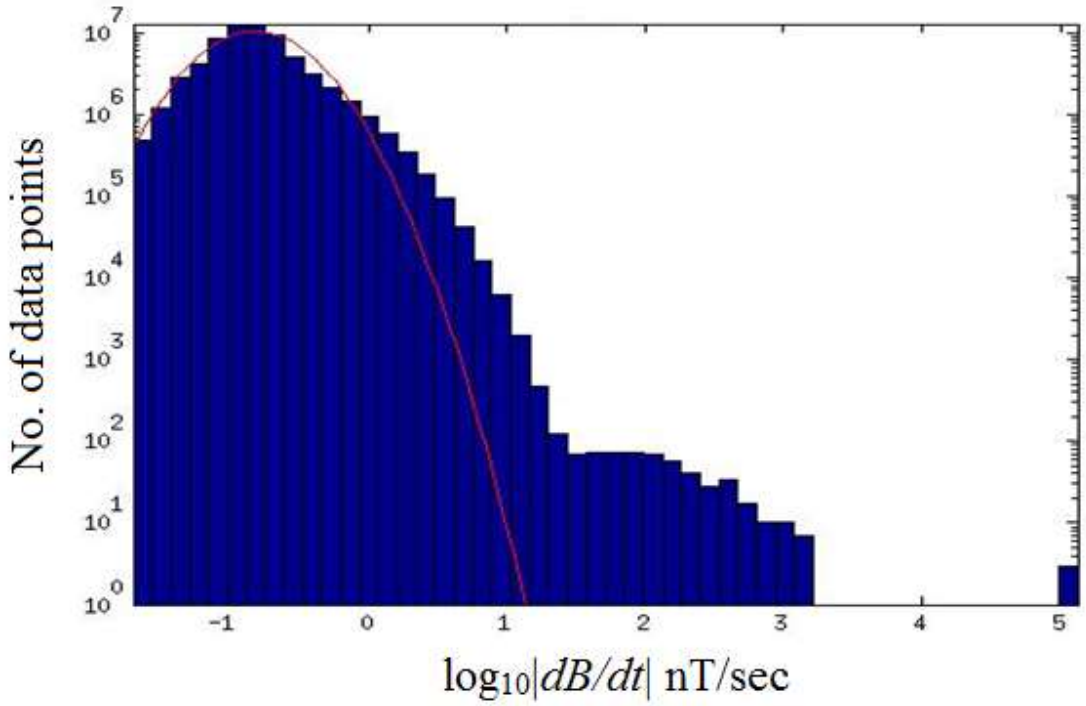

Figure 2.14: Histogram of the KJPK $\log_{10}|dB/dt|$ data with the best-fit lognormal distribution.

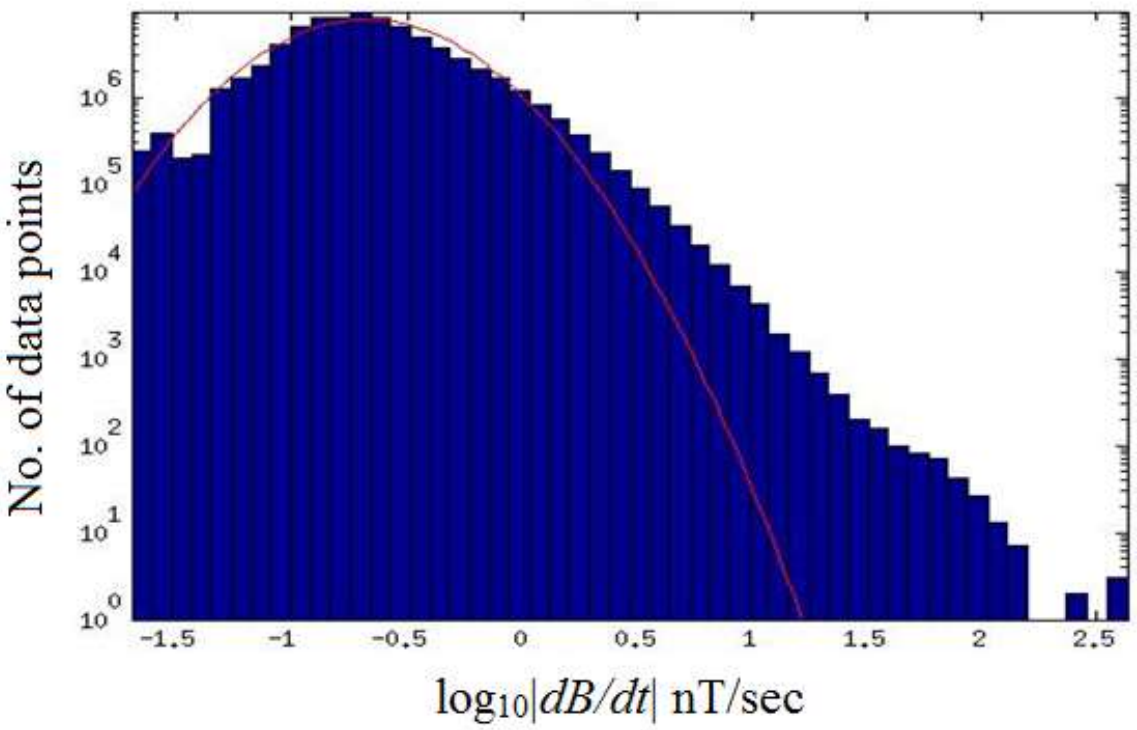

Figure 2.15: Histogram of the PUVR $\log_{10}|dB/dt|$ data with the best-fit lognormal distribution.

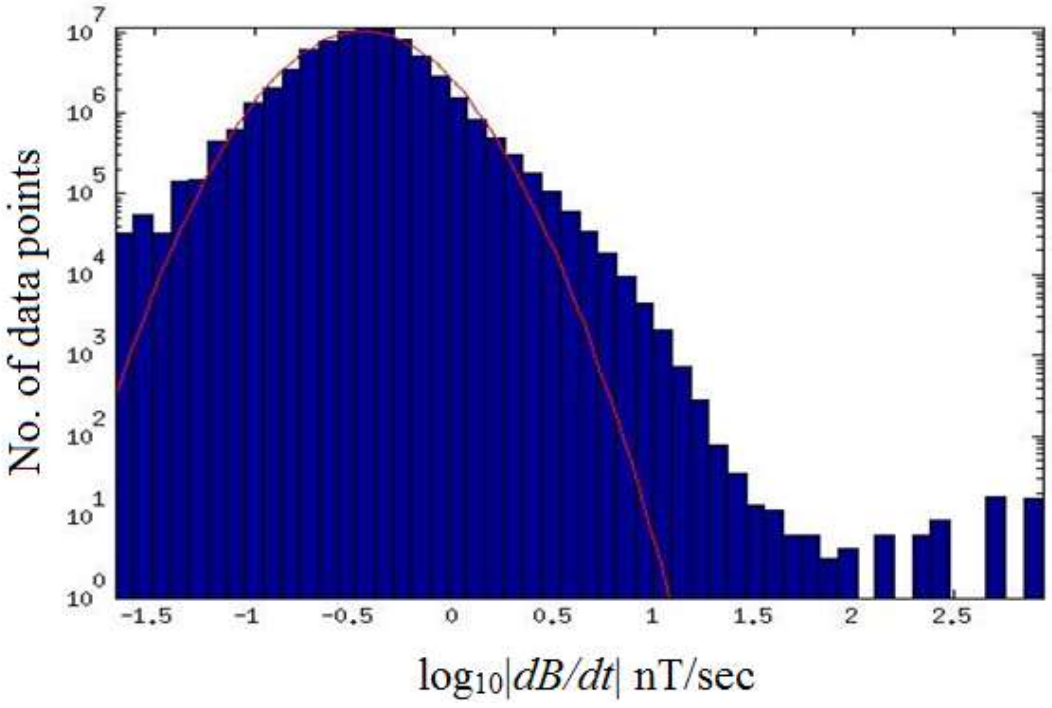

Figure 2.16: Histogram of the SALU $\log_{10}|dB/dt|$ data with the best-fit lognormal distribution.

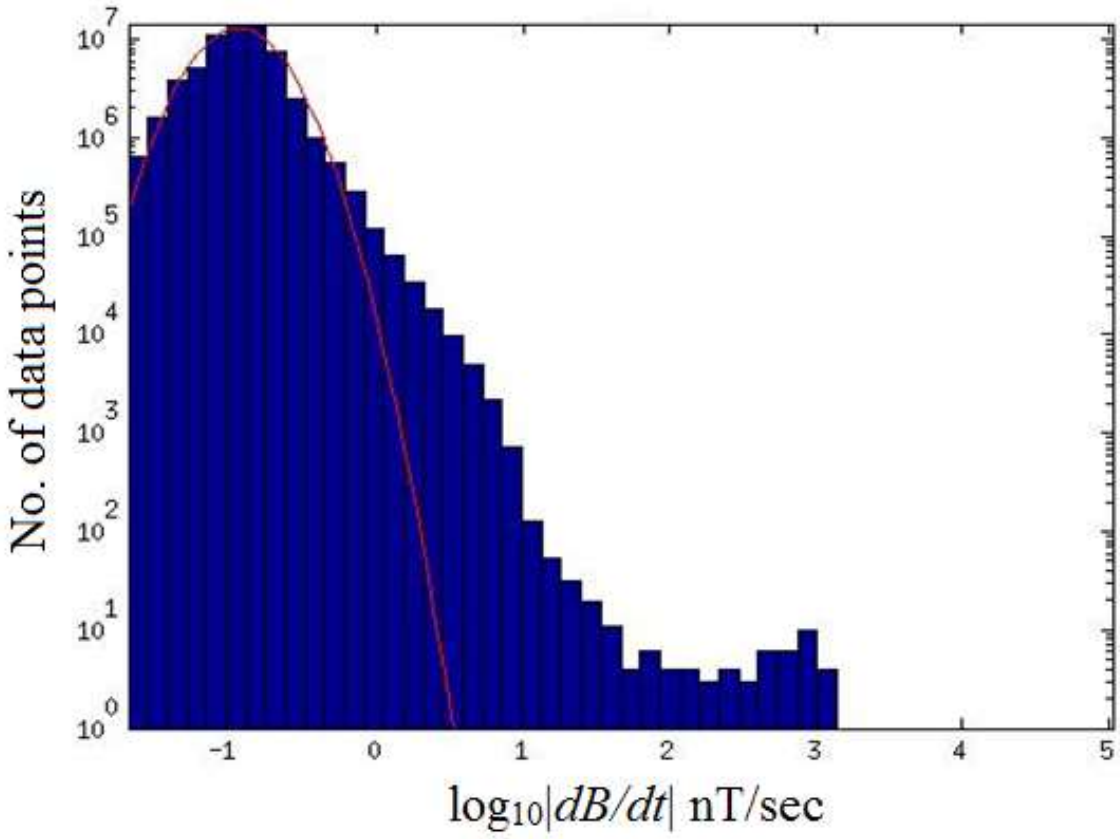

Figure 2.17: Histogram of the SEPT $\log_{10}|dB/dt|$ data with the best-fit lognormal distribution.

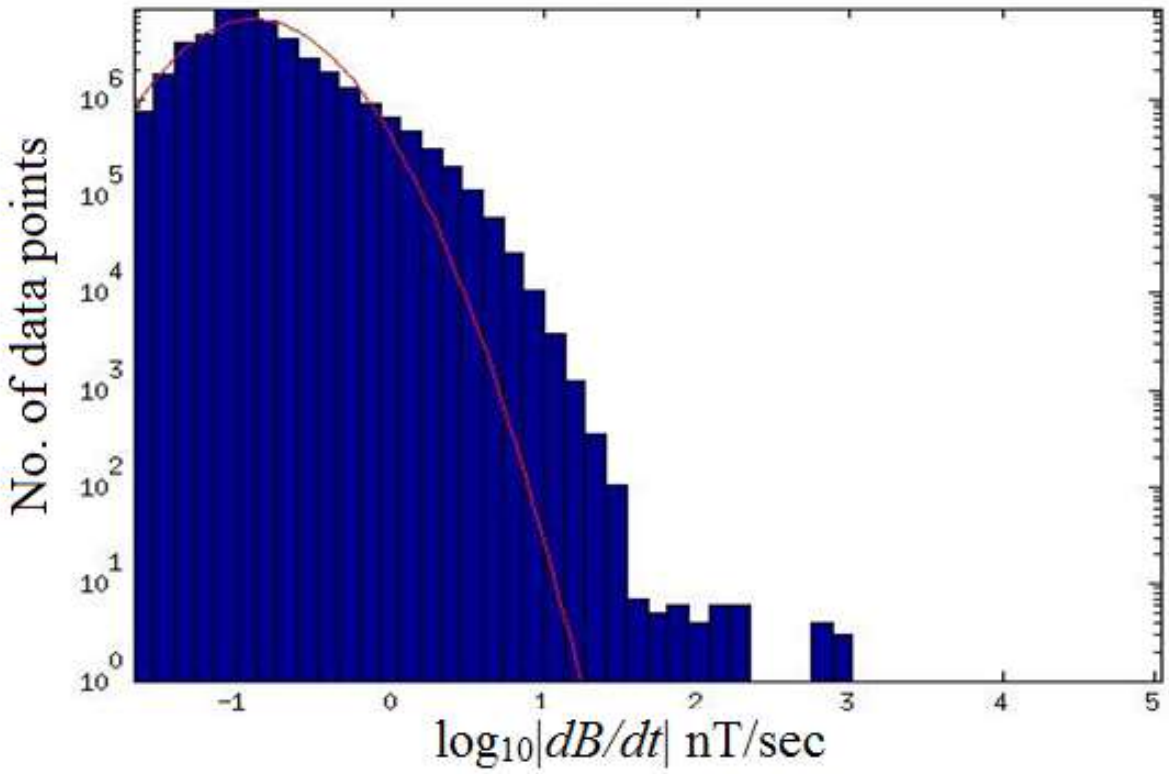

Figure 2.18: Histogram of the SCHF $\log_{10}|dB/dt|$ data with the best-fit lognormal distribution.

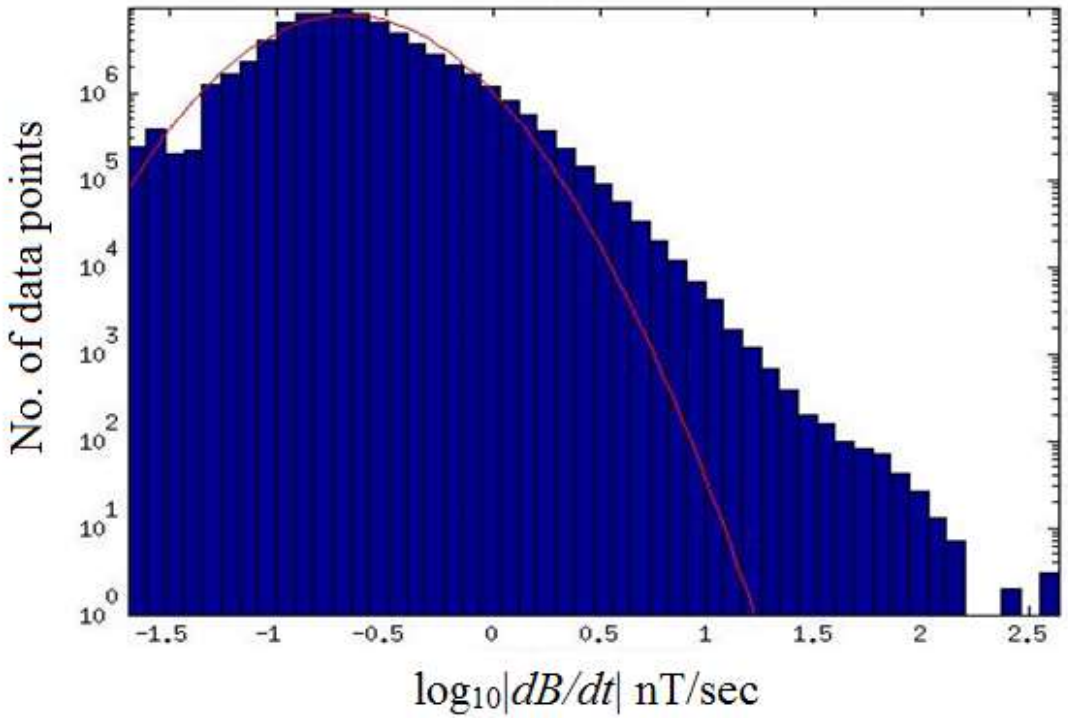

Figure 2.19: Histogram of the VLDR $\log_{10}|dB/dt|$ data with the best-fit lognormal distribution.

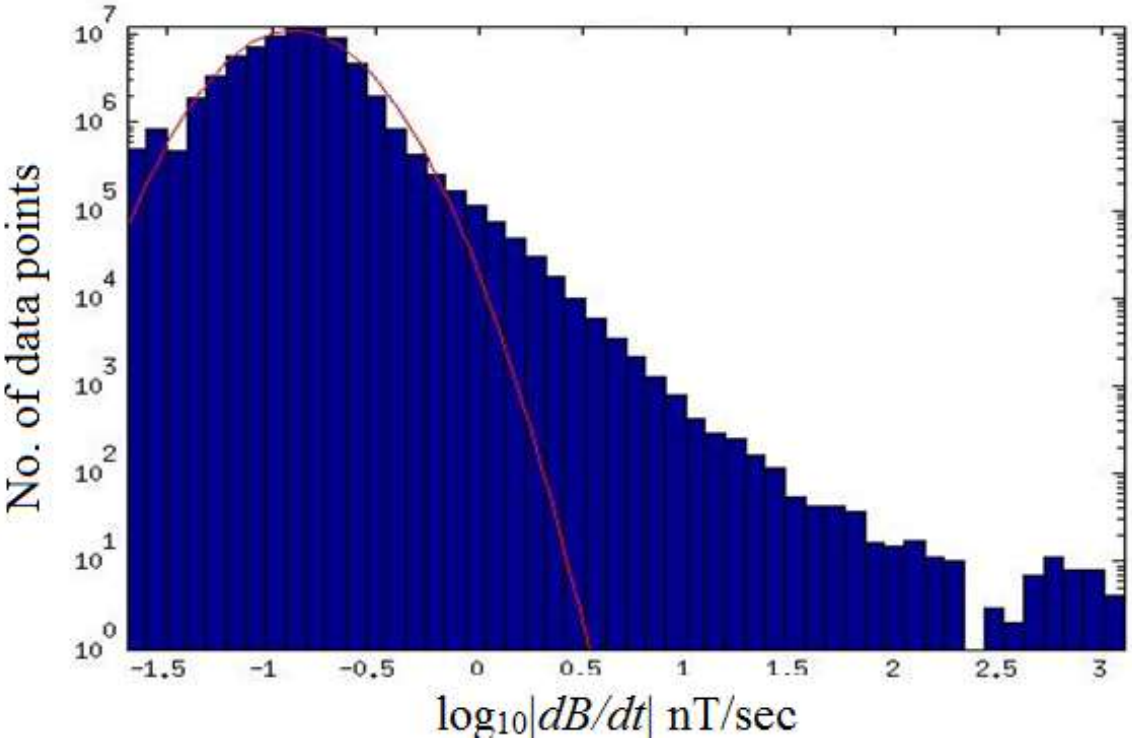

Figure 2.20: Histogram of the STFL $\log_{10}|dB/dt|$ data with the best-fit lognormal distribution.

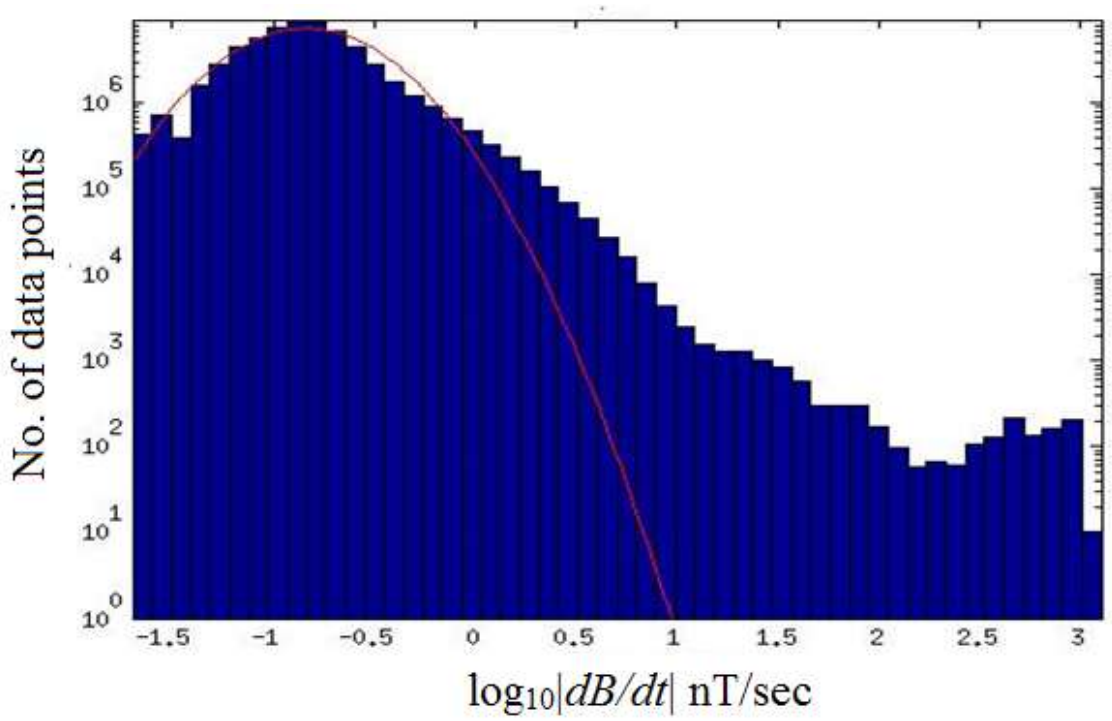

Figure 2.21: Histogram of the RADI $\log_{10}|dB/dt|$ data with the best-fit lognormal distribution (including erroneous data due to rest error).

2.3 Comparison of results from the AUTUMNX stations

Figure 2.22 shows the distribution of $\log_{10}|dB/dt|$ for all stations of the AUTUMNX array for Oct. 4, 2014 to Dec. 22, 2015. As expected, the northern stations situated at higher latitudes such as KJPK and AKUL have the maximum values of $\log_{10}|dB/dt|$ and experience greater changes in the geomagnetic field compared to stations at lower latitudes. The areas under the $\log_{10}|dB/dt|$ curves represent the amount of data used for the study. As SCHF was the last magnetometer to be installed, it has the least amount of data. The northern stations SALU, AKUL, and KJPK have higher values of $\log_{10}|dB/dt|$ and the values decrease moving towards the equator. This verifies the theory of higher latitude stations being more prone to GMDs [15].

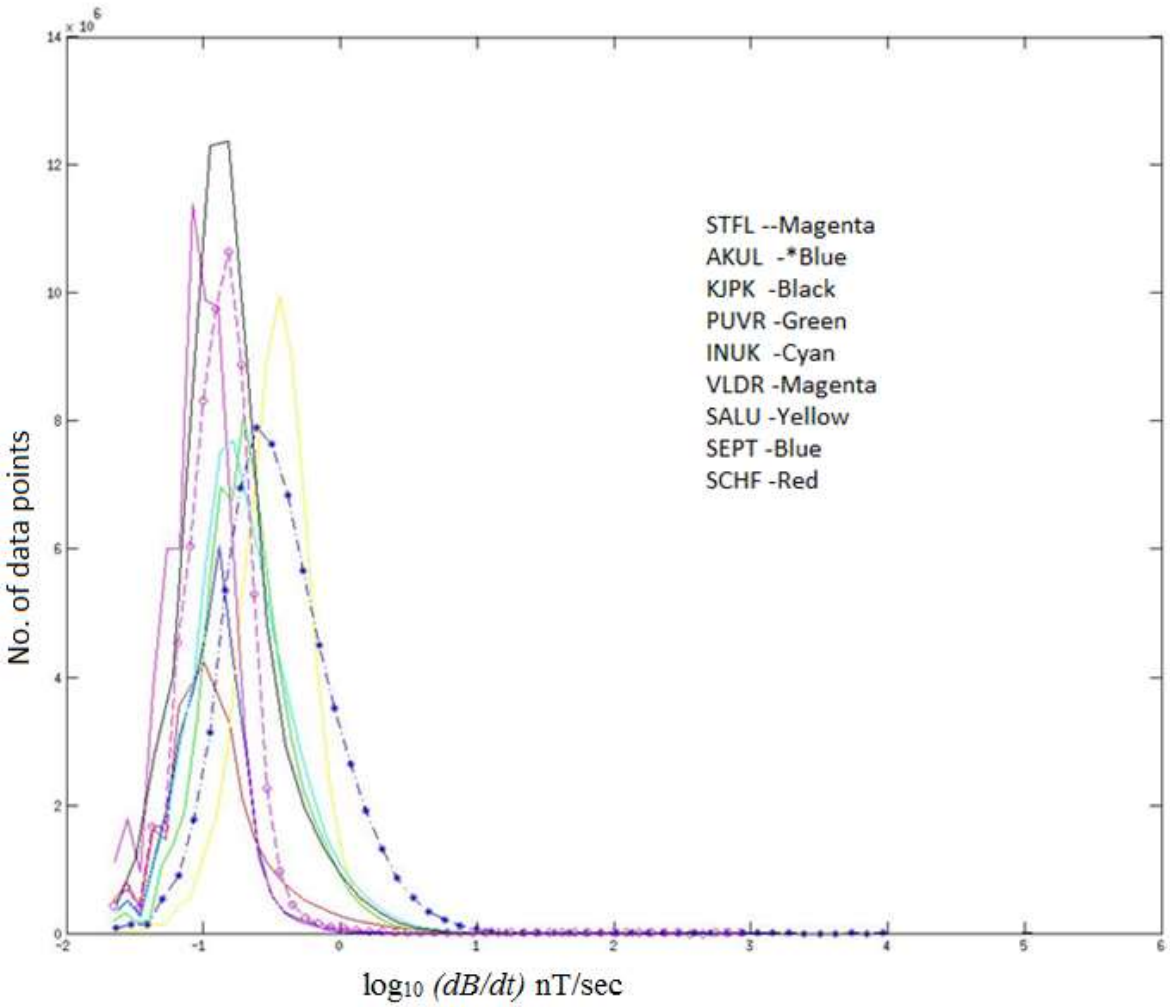

Figure 2.22: Distribution of $\log_{10}|dB/dt|$ for all stations of the AUTUMNX array for Oct. 4, 2014 to Dec. 22, 2015.

AUTUMNX station name	Mean of $\log_{10}\lvert dB/dt\rvert$ μ	SD of $\log_{10}\lvert dB/dt\rvert$ σ	Location
SALU	-0.46	0.27	latitude: 62.20 longitude: -75.65
AKUL	-0.44	0.41	latitude: 60.82 longitude: -78.15
PUVR	-0.68	0.34	latitude: 60.05 longitude: -77.29
INUK	-0.70	0.38	latitude: 58.47 longitude: -78.08
KJPK	-0.82	0.35	latitude: 55.28 longitude: -77.76
RADI	-0.84	0.32	latitude: 53.79 longitude: -77.62
VLDR	-1.03	0.25	latitude: 48.05 longitude: -77.78
STFL	-0.90	0.25	latitude: 48.65 longitude: -72.45
SEPT	-0.95	0.26	latitude: 50.22 longitude: -66.27
SCHF	-0.91	0.38	latitude: 54.80 longitude: -66.81

Table 1: The mean and standard deviation of $\log_{10}\lvert dB/dt\rvert$ for the AUTUMNX stations for the time period from Oct. 4, 2014 to Dec. 22, 2015.

AUTUMNX station name	Maximum of $\log_{10}\lvert dB/dt\rvert$	Date of occurrence of maximum of $\log_{10}\lvert dB/dt\rvert$
SALU	2.95	Oct. 3, 2015
AKUL	4.02	Jul. 22, 2015
PUVR	2.64	Oct. 29, 2014
INUK	3.14	Oct. 25, 2015
KJPK	5.12	Jun. 3, 2015
RADI	3.10	Nov. 10, 2015
VLDR	3.08	Mar. 13, 2015
STFL	3.10	Dec. 2, 2015
SEPT	5.03	Dec. 22, 2015
SCHF	5.04	Dec. 22, 2015

Table 2: The maximum values of $\log_{10}\lvert dB/dt\rvert$ for all AUTUMNX stations except RADI.

Table 1 gives the mean and standard deviation during the period of study from Oct. 4, 2014 to Dec. 22, 2015. These values help in identifying extreme geomagnetic activity due to a GMD event. The higher mean values for the northern latitude stations like AKUL indicate that they are more vulnerable to geomagnetic activity. Table 2 gives the maximum values of $\log_{10}\lvert dB/dt\rvert$ for all stations on a geomagnetically active day. SEPT and SCHF have maximums occurring on the same day at around the same time because the two sites are close to each other.

2.4 Comparison with the results in [1]

The histograms of $\log_{10}|dB/dt|$, intensity, variability and autocorrelation have a similar order of magnitude to those based on the CANOPUS data for the Gillam station presented in [1]. Thus, this report not only verifies the results in [1] but also the correctness of the results obtained from the AUTUMNX data. Figure 2.23 gives the histogram of $\log_{10}|dB/dt|$ over one day of CANOPUS data for Apr. 2, 2000. The dashed lines indicate the two best-fit lognormal distributions given in [1]. Discrepancies at the left side reflect instrumental (magnetometer) limitations and ambient noise. These results are very similar to Figures 2.8 to 2.10 for the SALU station data in terms of the peak geomagnetic activity observed in both cases ranging are from -1 to 1 along the *X*-axis. The maximum numbers of data points are of the same order 10^4 in both cases.

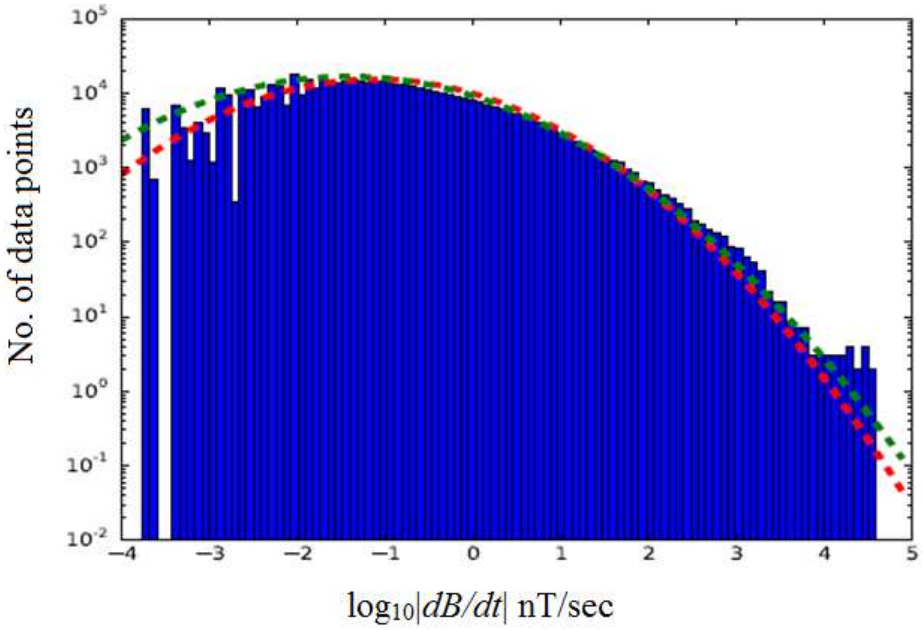

Figure 2.23: Histogram of $\log_{10}|dB/dt|$ for the Gillam station data from Apr. 2, 2000 [1].

Figure 2.24 shows the mean and standard deviation of $\log_{10}|dB/dt|$ calculated over 2.5 minute intervals for the CANOPUS data from Apr. 2, 2000. The variability has a nearly constant average with mostly noise-like variations. Figure 2.25 for the Gillam station from [1] is similar to Figure 2.9 in terms of the magnitude and shape of the results for the SALU station as the

average variability for both is around 0.25 nT per sec and the peak of the intensity is just above 0.5 nT per sec.

Figure 2.25 shows the autocorrelation of the intensity and variability for the Gillam station given in [1]. This is similar to the autocorrelation results obtained in Figure 2.10 from the SALU data. The variability has a very short correlation time (< 5 minutes), while the intensity is correlated over timescales of tens of minutes to hours.

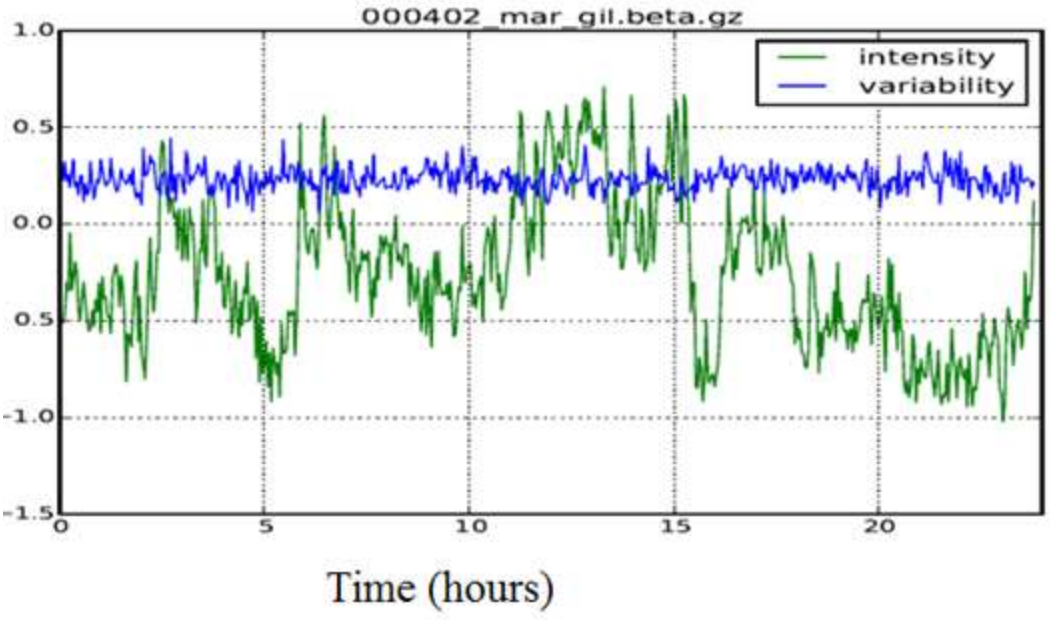

Figure 2.24: Intensity and variability for the Gillam station data from Apr. 2, 2000 [1].

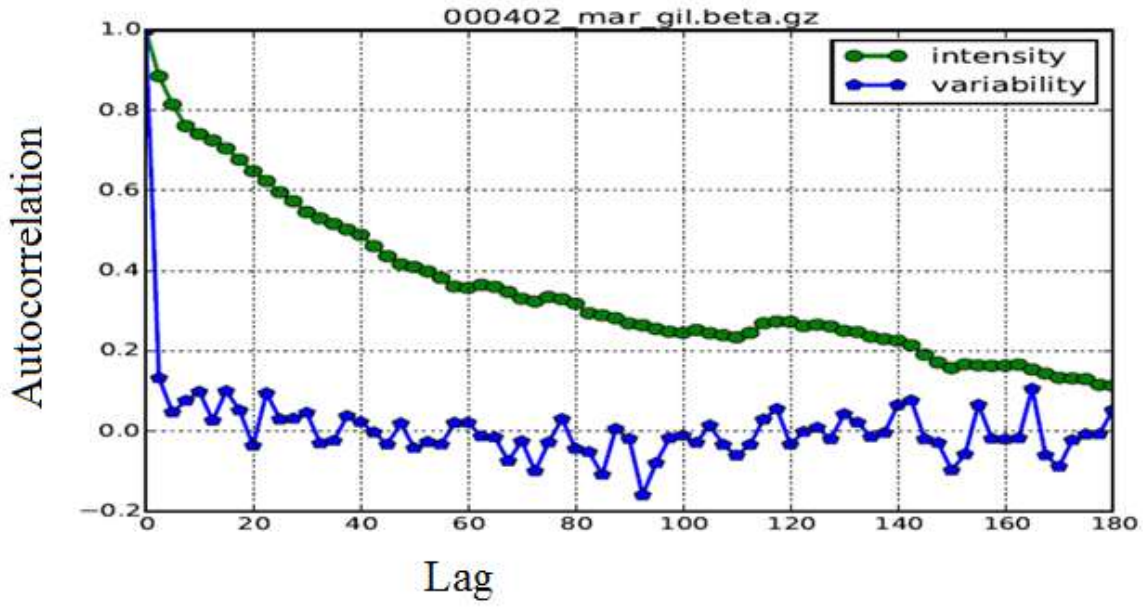

Figure 2.25: Autocorrelation of the intensity and variability calculated over 2.5 minute intervals for the Gillam station data from Apr. 2, 2000 [1].

2.5 Discussion

Instrument errors can affect the data and produce biased results. A vehicle passing by a magnetometer and magnetometer reset can introduce false values which are not linked to a geomagnetic storm. The RADI station had many such instances. Sometimes a magnetometer can have a malfunction and display arbitrary symbols instead of numbers for the magnetic field values. Physical factors like the weather may affect magnetometer operation which in turn leads to missing data in the online system. In some cases, a machine malfunction can halt the magnetometer from working, and only after the machine is repaired can it function normally. A reset in the system can lead to absurd values in the data, e.g. negative infinity, positive infinity and not a number (NaN) values were found and discarded during analysis of the AUTUMNX data. These erroneous values were removed from the data sets to obtain the results.

Magnetometer reset error and GPS issues can cause false abnormal spikes which skew the distributions. These can be identified by comparing results from different stations. If a spike is seen at only one station it signifies a reset error. A large amount of data can take a long time to process. It can also lead to storage issues due to the limited hard disk space available. The MAT files function in MATLAB resolved these problems to quite an extent. In addition, pre-allocating

memory to the variables reduced the execution time so it only took a few hours to process years of data instead of days.

2.6 Hydro-Quebec harmonic data analysis

Figure 2.26 shows the maximum harmonic distortion (HD) data in per unit (pu) for the ten Hydro-Quebec substations. Comparing results obtained from the Hydro-Quebec harmonic distortion (HD) data in Figure 2.26 to the MACCS and AUTUMNX results in Figure 2.27, one can establish that the change in the magnetic field due to geomagnetic storms is the prime cause of the large harmonics seen in the Hydro-Quebec power system. In both figures, the majority of the activity is seen around midnight local time. The change in magnetic field is reflected in the power system as the harmonics are induced around the same time. Figure 2.28 shows the difference between successive values of B for all three directional components (ΔB_X, ΔB_Y, and ΔB_Z) versus coordinated universal time (UTC) on separate plots unlike Figure 2.28 where all are shown on the same plot. These plots were generated to identify which directional component of the magnetic field is dominant. They also help in identifying the direction of the solar wind and thus the direction of the GICs.

Figure 2.29 shows the average (of the three phases of Voltage) of the even harmonic distortion (EHD) for various Hydro-Quebec substations (BOU, CHA, CHI, CHU, LG2, MIC, NIC, OUT, RIM and TIL) versus time [17]. This data was collected from a real-time system, Système de Mesure de Décalage Angulaire (SMDA), installed to monitor voltage harmonic distortion at different Hydro-Quebec substations. Even harmonics data is useful for geomagnetic activity detection [18]. In Figure 2.29, TIL has the highest harmonic content, for instance, when the other stations are below .005 (0.5%) harmonic distortion, TIL is over .01 (1%) harmonic distortion. The reason for the high level of activity is its location (geology and in the auroral zone) and also due to the power network configuration. TIL is connected through a 315 KV transmission line without series compensation.

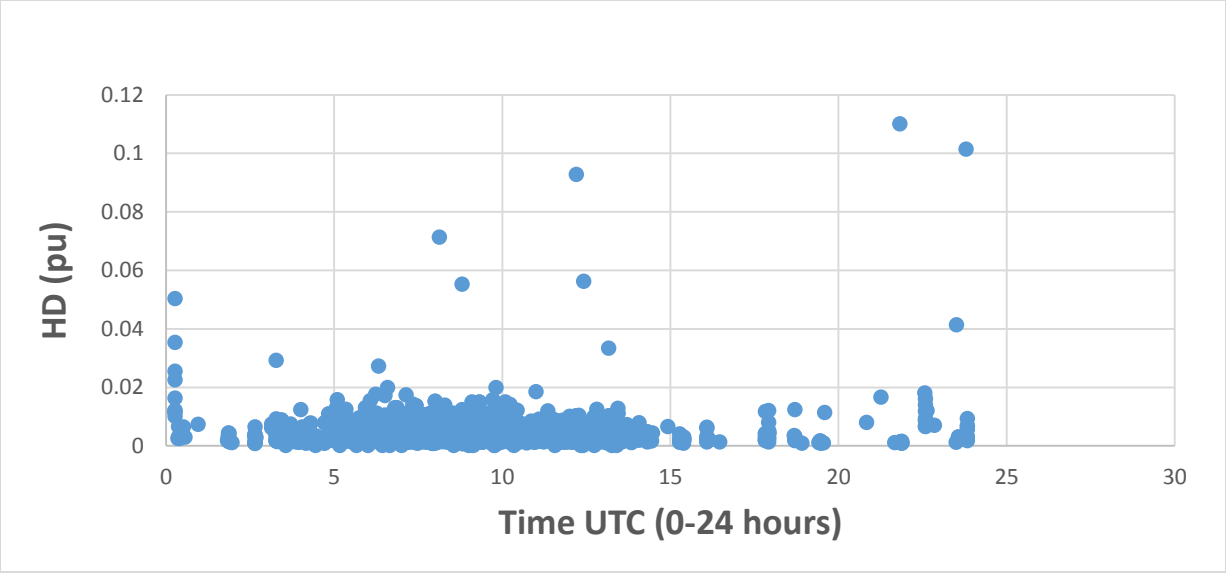

Figure 2.26: Average even harmonic distortion for all Hydro Quebec substations versus time [16].

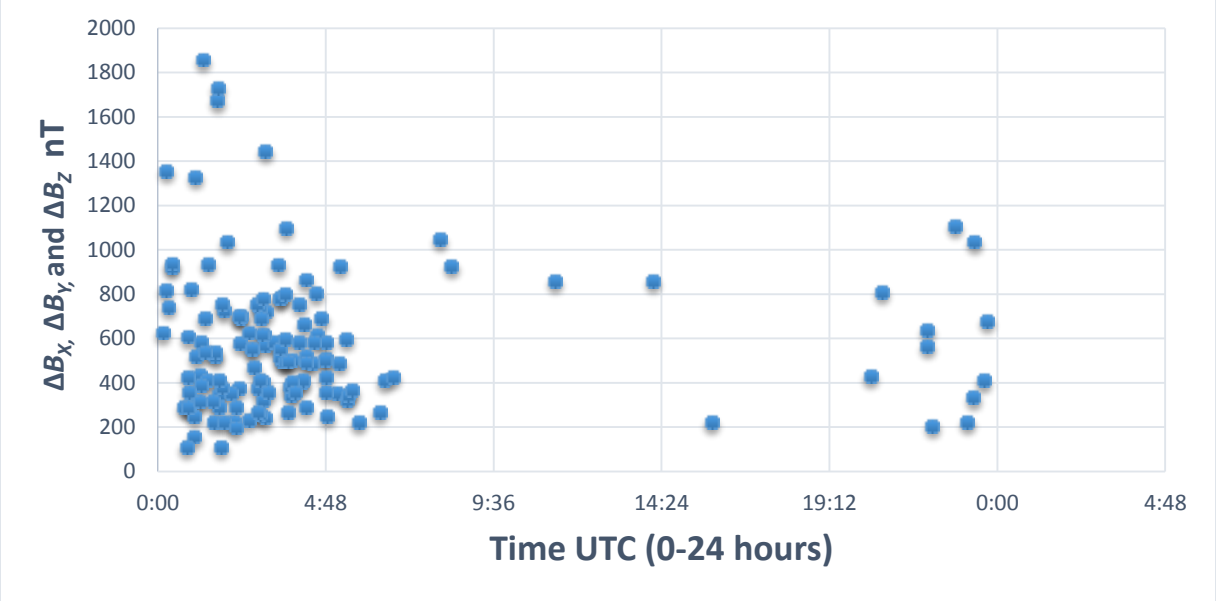

Figure 2.27: Change in magnetic field for all three components *X*, *Y* and *Z* versus time in UTC (coordinated universal time) from Jul. 1, 2014 to May 1, 2017 [16].

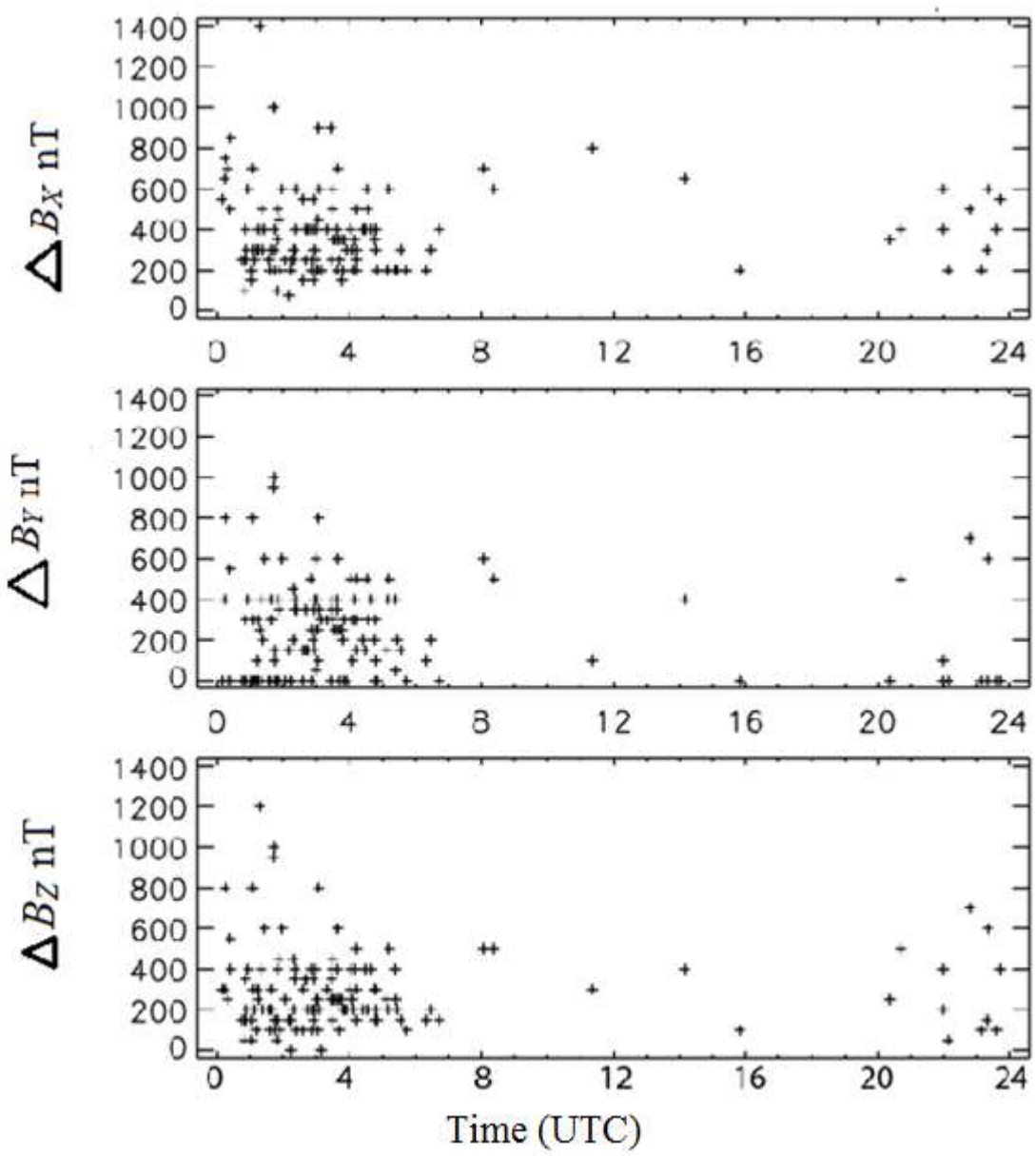

Figure 2.28 AUTUMNX and MACCS data, ΔB_X, ΔB_Y, and ΔB_Z versus time (UTC) for Jul. 1, 2014 to May 1, 2017 [16].

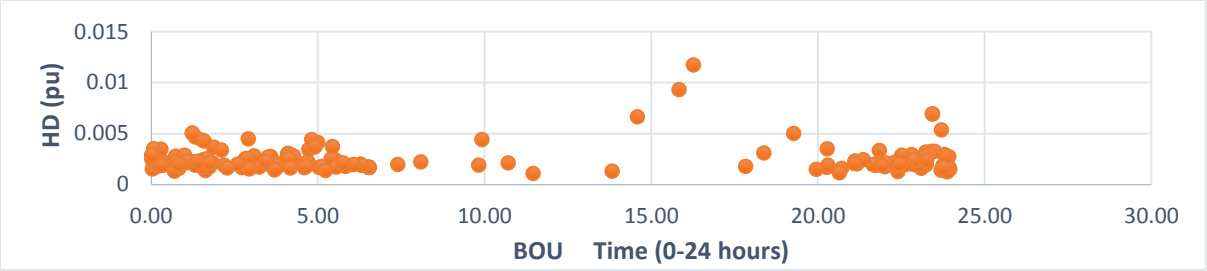
HD (pu)
0.015
0.01
0.005
0
0.00
5.00
10.00
15.00
20.00
25.00
30.00
BOU Time (0-24 hours)

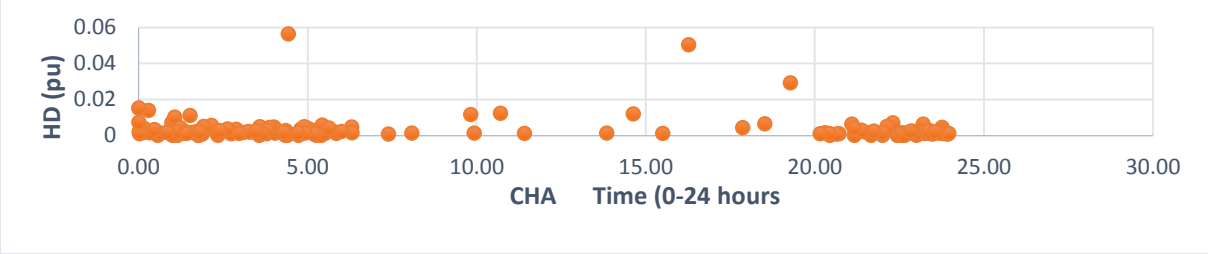
HD (pu)
0.06
0.04
0.02
0
0.00
5.00
10.00
15.00
20.00
25.00
30.00
CHA Time (0-24 hours

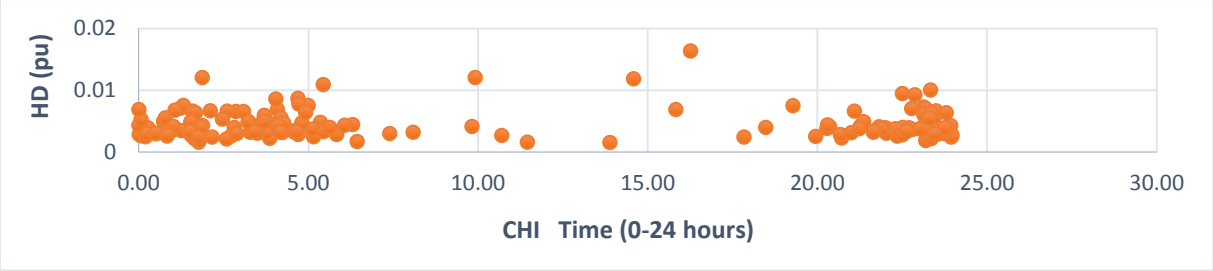
HD (pu)
0.02
0.01
0
0.00
5.00
10.00
15.00
20.00
25.00
30.00
CHI Time (0-24 hours)

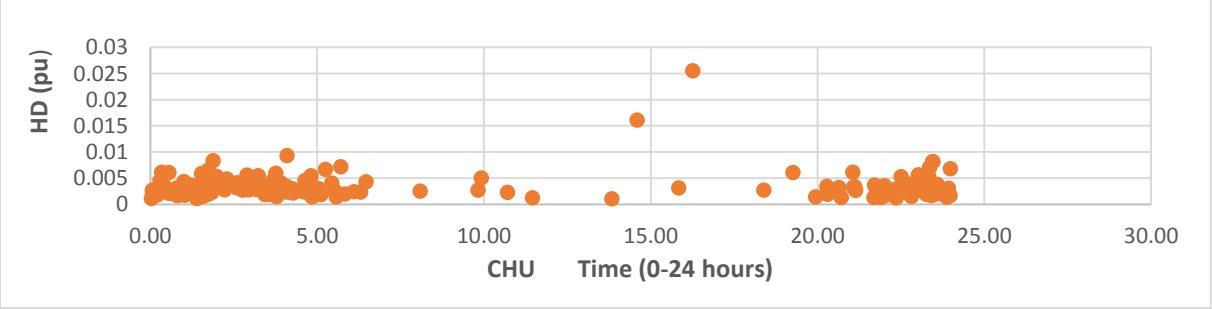
HD (pu)
0.03
0.025
0.02
0.015
0.01
0.005
0
0.00
5.00
10.00
15.00
20.00
25.00
30.00
CHU Time (0-24 hours)

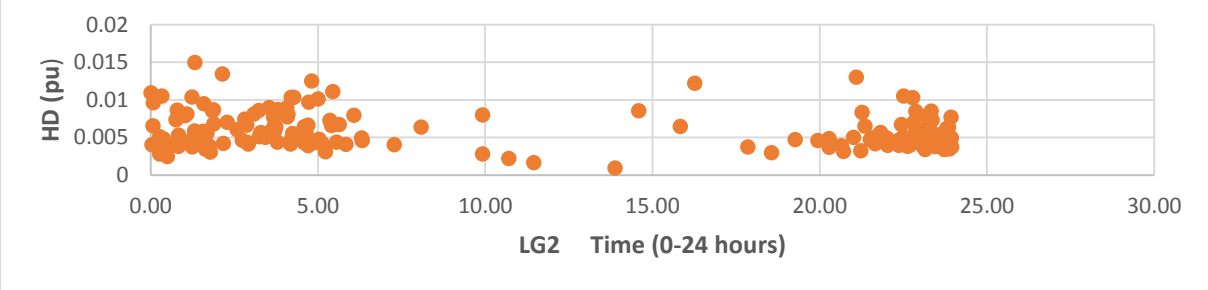
HD (pu)
0.02
0.015
0.01
0.005
0
0.00
5.00
10.00
15.00
20.00
25.00
30.00
LG2 Time (0-24 hours)

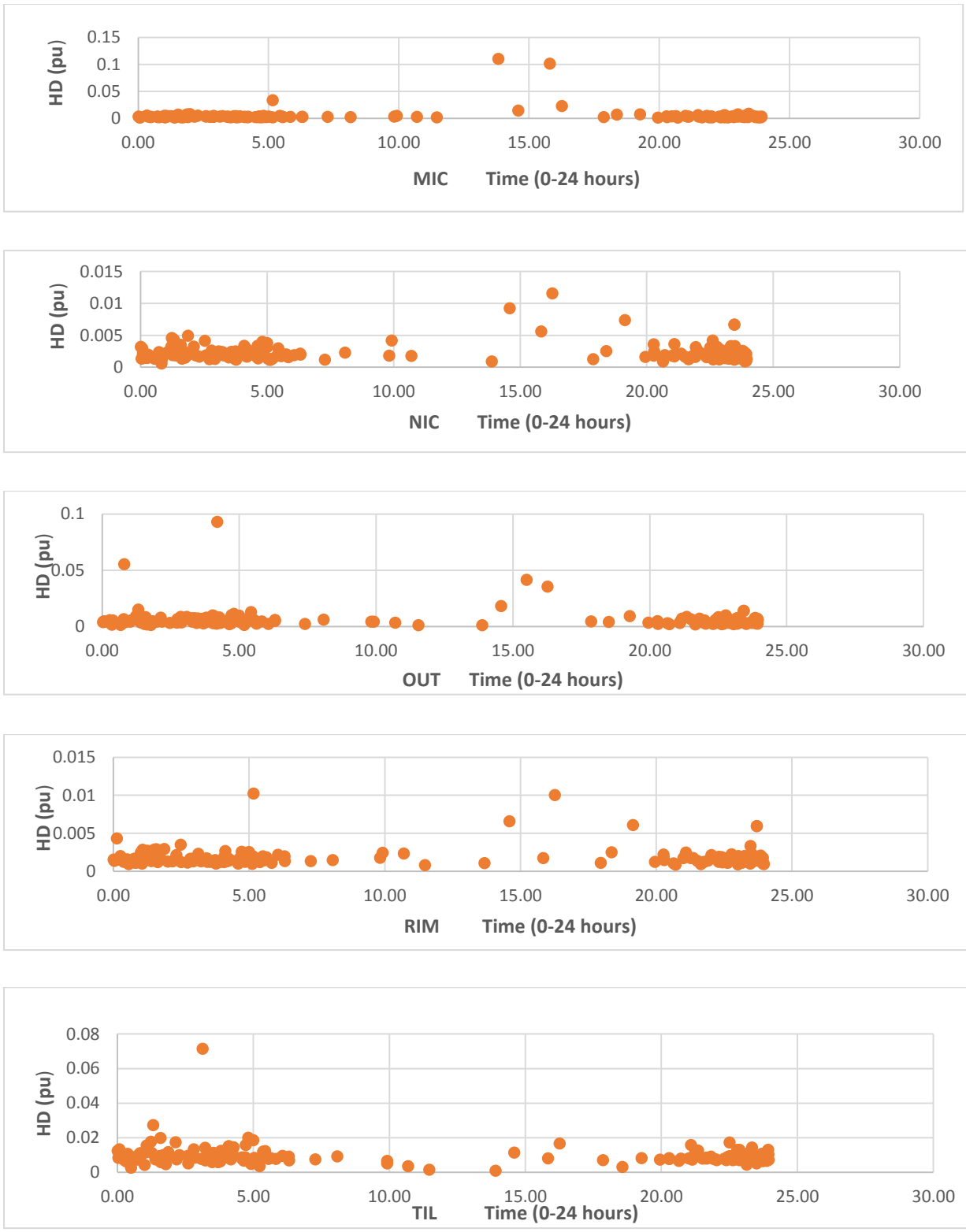

Figure: 2.29 Average even harmonics distortion (HD) for various Hydro-Quebec substations versus time (UTC) [17].

Chapter 3: Conclusions and future work

The results obtained from the AUTUMNX data in this report were used to verify the results of the CANOPUS data in [1]. These results are consistent with a lognormal distribution and can be used for quantitative predictions. Comparing the Hydro-Quebec data with the AUTUMNX data results verified that considerable harmonics are induced by GMDs. Due to insufficient awareness in the past many GIC related issues were not attributed to GMDs. Thus, this work can help utilities identify GIC induced problems in their power systems. During analysis of the AUTUMNX data, problems related to the quality of data were discovered and conveyed to the researchers. This helped the AUTUMNX research team repair the magnetometer at the RADI station which was giving erroneous data.

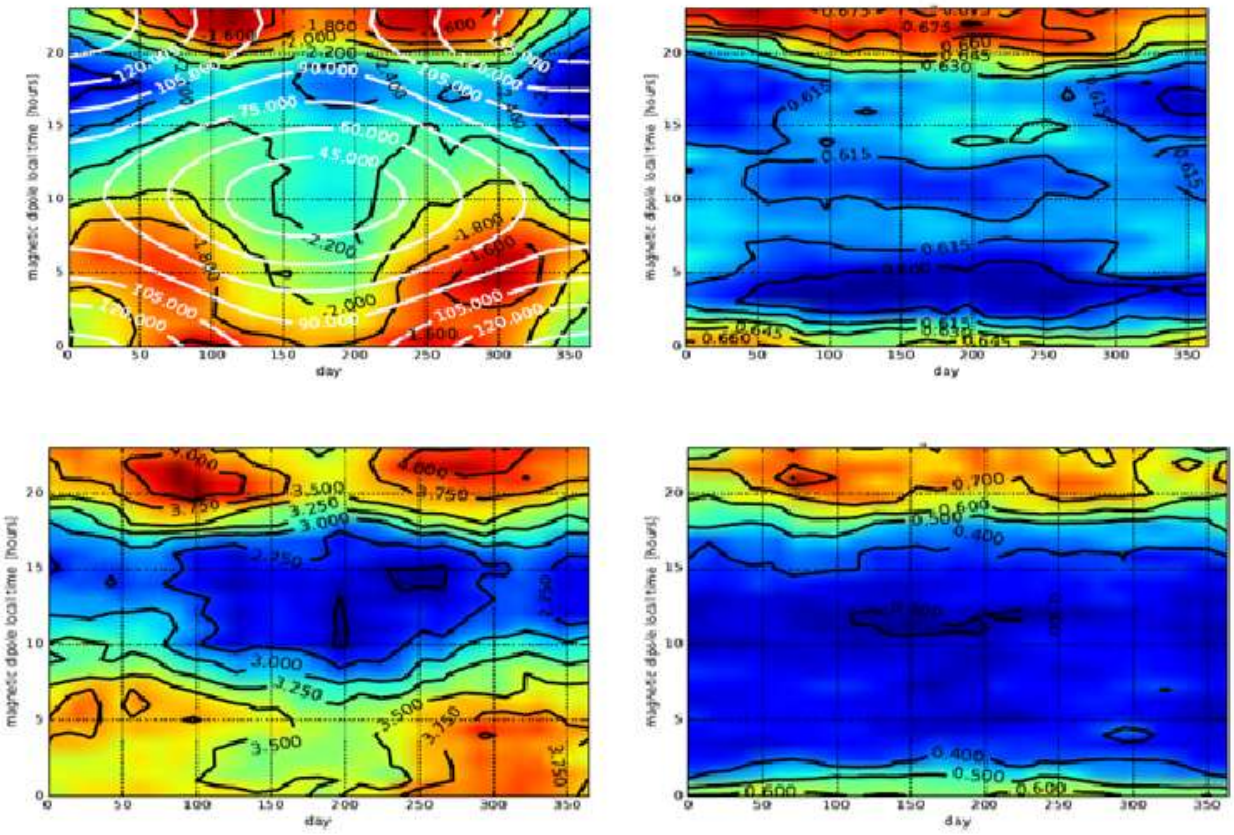

Figure 3.1: Results for local time and seasonal variations of intensity and variability [1].

The next step of this study would be to plot intensity and variability for one year of data. In addition, verify the second part of the analysis given in [1] by producing results based on seasonal variation as shown in Figure 3.1. This report also forms the basis for work related to intensity versus solar wind as in [1]. This may help researchers predict extreme events based on time and seasonal variations. The statistical approach can be very useful for scientists to predict the occurrence of events and study the pattern of events, for example, aid Hydro-Quebec in predicting GICs and plan risk mitigation techniques to avoid events like the 1989 blackout.

Bibliography

1. B. J. Jackel, M. Connors, K. Reiter, “Predicting lognormal distributions of geomagnetic time derivatives”, in preparation.
2. R. Fazio, L. Marti, Hydro One, “Power quality”, large customer conference, Sept. 2014.
3. W. Whitson, “Geomagnetic disturbances (GMD), causes and effect on the North American systems”, Presentation (ppt), Apr. 2012.
4. Natural Resources of Canada, space weather Canada, (http://www.spaceweather.gc.ca/tech/se-pow-en.php).
5. J. Kappenman, Metatech Corporation, American association for the advancement of science press briefing, Advanced geomagnetic storm forecasting capabilities developed for the electric power industry, Feb. 2000.
6. S. Guillon, P. Toner, L. Gibson, D. Boteler, “A colorful blackout”, IEEE Power and Energy Magazine, vol. 14, issue 6, pp. 59-71, Dec. 2016.
7. L. Marti, "Effects of series compensation capacitors on geomagnetically induced currents", IEEE transactions on power delivery, vol. 29, issue 4, pp. 2032-2033, Aug. 2014.
8. D.H. Boteler, R.J. Pirjola, H. Nevanlinna, “The effects of geomagnetic disturbances on electrical systems at the earth's surface”, Advances in space research, vol. 22, issue 1, pp. 17-27, Sept. 1998.
9. AUTUMN virtual magnetic observatory, (http://autumn.athabascau.ca/).
10. IAGA ASCII exchange format, (www.ngdc.noaa.gov/IAGA/vdat/IAGA2002/iaga2002format.html).
11. M. Connors et al., “The AUTUMNX magnetometer meridian chain in Quebec, Canada”, earth, planets and space, Springer New York, Jan. 2016.
12. Lognormal distribution, mathworks.com, (https://www.mathworks.com/help/stats/lognormal-distribution.html).
13. P. L. Menezes et al., Tribology for scientists and engineers, from basics to advanced concepts, Springer-Verlag New York, 2013.
14. Autocorrelation function, mathworks.com, (https://www.mathworks.com/help/econ/autocorr.html?s_tid=doc_ta).

15. Peak Reliability- Geomagnetic disturbance operating plan, version 3.1, NERC standard EOP-0101, (www.peakrc.com/RCDocs/GMD%20Operating%20Plan%20v3.1.pdf).
16. M. Engebretson, M. Connors, J. Posch, D. Braun, “High latitude magnetic impulse events in the evening sector in eastern North America”, Jun. 2017, private communication.
17. S. Guillon, Hydro-Quebec data, Jun. 2017, private communication.
18. C. Deguire, “Phasor measurement Hydro-Québec TransÉnergie”, North American Synchrophasor Initiative (NASPI), Environmental, Social and Corporate Governance (ESG), Feb. 2007.